SLIDING-MODE CONTROL OF DC–DC BOOST CONVERTER WITH CONSTANT IMPEDANCE AND CONSTANT POWER LOADS

by

HanQing Lin

B.A.Sc., The University of British Columbia, 2013

A THESIS SUBMITTED IN PARTIAL FULFILLMENT OF

THE REQUIREMENTS FOR THE DEGREE OF

MASTER OF APPLIED SCIENCE

in

THE FACULTY OF GRADUATE AND POSTDOCTORAL STUDIES

(ELECTRICAL AND COMPUTER ENGINEERING)

THE UNIVERSITY OF BRITISH COLUMBIA

(Vancouver)

October 2020

The following individuals certify that they have read, and recommend to the Faculty of Graduate and Postdoctoral Studies for acceptance, a thesis entitled:

Sliding-Mode Control of DC–DC Boost Converter with Constant Impedance and Constant Power Loads

submitted by HanQing Lin in partial fulfillment of the requirements for

the degree of Master of Applied Science

in Electrical and Computer Engineering

Examining Committee:

Dr. Juri Jatskevich, Electrical and Computer Engineering
Supervisor

Dr. Ryozo Nagamune, Mechanical Engineering
Supervisory Committee Member

Dr. Christine Chen, Electrical and Computer Engineering
Supervisory Committee Member

Abstract

An essential component in modern DC systems is the bus-forming boost converter. However, voltage regulation of the boost converter in continuous conduction mode using traditional linear technique is not an easy task due to the system's inherent right-half-plane zero, which often forces designers to settle with a controller that has narrow bandwidth and poor dynamic response in exchange for adequate stability margin. The effectiveness of linear controllers is further undermined by the nonlinearities of the system. To address these limitations, sliding-mode control, which is a nonlinear control method well-known for its intrinsic stability, robustness and fast response, has gained increased attention in its application to DC–DC boost converters.

This thesis focuses on the theoretical analysis as well as the practical implementation of sliding-mode control for boost converters supplying constant impedance and constant power loads. The first part of this thesis reviews the conventional sliding-mode controller for boost converters with simple resistive load and identifies its drawback, whereupon an observer-based fixed-frequency sliding-mode controller is proposed to improve output response while keeping sensor count low. The second part of this thesis extends the basic framework of sliding-mode control to boost converters supplying both constant impedance and constant power loads. The nonlinear mixed-load system is analyzed rigorously, and an accurate closed-loop small-signal model is derived, giving insight into system dynamics and stability. The third part of this thesis utilizes the results from the analysis of the mixed-load system and proposes a new adaptive sliding-mode controller to improve system performance while guaranteeing stability. Simulation studies and experimental results are included to support the analysis and validate the proposed control

strategies. The analytical approach presented here is sufficiently general that it may be applied to other converter typologies. The proposed control strategies provide new and beneficial alternatives for power electronic design engineers who are seeking fast, stable and robust control solutions.

Lay Summary

Sliding-mode control is an advanced control method that is fast, stable and easy to implement. It is suitable for controlling power electronic converters, especially the DC-DC boost converter which is at the heart of today's rapidly-growing DC systems. This thesis studies sliding-mode control for boost converters supplying different types of loads, and proposes new control strategies to improve upon the existing state-of-the-art for faster and more stable operation. The analytical technique presented here can be extended to other types of converter systems under sliding-mode control. The proposed control strategies offer new and beneficial alternatives for power electronic design engineers.

Preface

The research presented in this thesis has resulted in two IEEE conference papers. As the first author of both papers, I originated the ideas and methods, performed the theoretical analysis, conducted simulation studies and experiments, and prepared the manuscripts. My research supervisor, Dr. Juri Jatskevich, outlined the research topic with me and provided valuable feedback on the manuscripts. Dr. Seyyedmilad Ebrahimi helped revise the manuscripts and provided critical comments. Mohammad Mahdavyfakhr provided useful discussions. The two conference papers stemming from this work are listed below.

Chapter 2 contains a modified version of the following conference paper that has been published:
H. Lin, S. Ebrahimi, M. Mahdavyfakhr and J. Jatskevich, "An Observer-Based Fixed-Frequency Sliding-Mode Controller for Boost Converters," in *Proc. 10th IEEE Annu. Inf. Technol. Electron. Mobile Commun. Conf. (IEMCON)*, Vancouver, BC, Canada, pp. 0270-0275, Oct. 2019.

Chapter 3 and 4 are based on the following conference paper, which has been accepted and will be presented at the upcoming conference in November:
H. Lin, S. Ebrahimi, M. Mahdavyfakhr and J. Jatskevich, "Analysis of Sliding-Mode-Controlled Boost Converters with Mixed Loads," at *21st IEEE Workshop Control Modeling Power Electron. (COMPEL)*, Nov. 2020.

The introductory Chapter 1 contains modified contents from both papers above.

Table of Contents

List of Tables

List of Figures

List of Abbreviations

AC	Alternating Current
ADC	Analog-to-Digital Converter
CCM	Continuous Conduction Mode
DC	Direct Current
DSP	Digital Signal Processor
HC	Hysteresis Controller
I/O	Input and Output
LPF	Low-Pass Filter
MCU	Microcontroller Unit
PI	Proportional-Integral
PWM	Pulse Width Modulation
SM	Sliding-Mode
SMC	Sliding-Mode Control

Acknowledgements

First of all, I want to express my deepest gratitude to Dr. Juri Jatskevich for giving me the opportunity to pursue a master's degree under his supervision. Over these two years, I was able to grow my knowledge in control and modeling — the two areas I need the most in my career — all thanks to Dr. Jatskevich's extensive expertise and kind encouragement. Despite the many challenges and restrictions we face due to the COVID-19 pandemic, Dr. Jatskevich's hard work, dedication and tenacity during this difficult time ensured the successful completion of my research and this thesis. For that, I'm deeply touched and extremely grateful.

I want to give my sincere thanks to Dr. Ryozo Nagamune and Dr. Christine Chen for dedicating their valuable time to serve on my examining committee and for all of their valuable feedback which has helped improve this thesis.

I want to thank Dr. Ryozo Nagamune, who taught the graduate course on control, for his excellent lectures and lecture notes, and for offering his valuable time to help with my questions. I also want to thank Dr. Martin Ordonez, who taught the graduate course on power electronics, for his stylish delivery in class and for introducing me to sliding-mode control. They have influenced my research in many ways.

I would like to give my appreciation to Dr. Seyyedmilad Ebrahimi for revising my papers and offering several critical comments both technical and style wise. I would also like to thank Mohammad Mahdavyfakhr for the companionship during our study and research at UBC.

I want to thank all the staffs at our ECE graduate office for their attentive, prompt support.

I want to thank my parents for their love and care.

Dedication

To my mother

Chapter 1: Introduction

The renewable resources such as solar, wind and tidal are widely adopted to harness energy; as a result, the electrical grid is rapidly transforming to incorporate these changes. The transportation sector is also experiencing massive shift as electric vehicles are becoming favored by consumers. Amidst this technological evolution, one key enabler is the advance of power electronics, where the DC-DC converters are the fundamental building blocks of many systems.

1.1 Overview of Power Electronic-Based DC Systems

High-frequency power electronic converters open the door for low-cost, high-efficiency and high-power-density solutions that penetrate modern DC systems, ranging from DC microgrids [1] to the on-board power systems of electric vehicles [2]. A typical setup of such systems is illustrated in Figure 1.1. Therein, the DC source can be from renewable resources such as solar or wind, or from a battery-based storage, which is usually stepped up by a boost-type DC–DC converter to produce a higher bus voltage. The electrical loads connected to the DC bus can comprise an assortment of resistive elements (such as heaters), DC–AC inverters (that may feed three-phase machines) and DC–DC converters (that may feed DC loads).

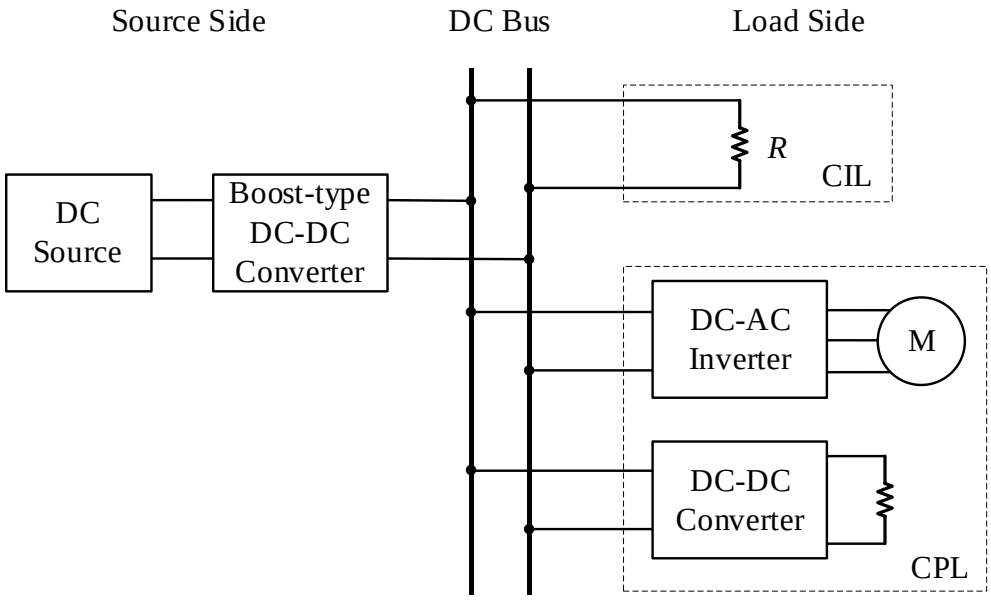

Figure 1.1 Simplified schematic of electrical systems commonly seen in DC microgrids and on-board power systems of electric vehicles.

1.2 Control of the Bus-Forming DC–DC Boost Converter

It is evident that the key element in Figure 1.1 is the bus-forming boost converter as the rest of the system relies on its capability to provide regulated output voltage even in the presence of input and load disturbances. However, two challenges emerge.

First, voltage regulation of the boost converter in continuous conduction mode (CCM) is difficult due to its innate characteristics. In the sense of classical control theory, the CCM boost converter is a non-minimum-phase system which is made evident by its right-half-plane zero in its control-to-output transfer function [3]. This poses a fundamental limit on what traditional linear controllers can achieve for this type of system, often resulting in a control loop of narrow bandwidth and poor dynamic response [3]. Additionally, since linear controllers are designed

around a certain operating point, their effectiveness is further undermined by the system's nonlinearities [4].

Second, as shown in Figure 1.1, loads attached to the DC bus do not only contain linear resistive elements, or constant impedance loads (CILs) (the term resistive load and CIL will be used interchangeably in the scope of this work); tightly-regulated loads, such as inverters and converters, behave like constant-power loads (CPLs) which are nonlinear and exhibit negative incremental resistance that can weaken or even destabilize the system [2]. The destabilizing effect of CPLs in DC systems has been studied extensively and continues to be a hot topic in the research community [5], [6]. The presence of CPLs further increases the complexity and difficulty in designing a fast and stable controller for the bus-forming boost converter.

1.3 Sliding-Mode Control of DC–DC Converters

To address the limitations of linear controllers, various nonlinear control techniques, such as fuzzy control [7] and sliding-mode (SM) control [8], have been developed. Their applications to DC-DC converters have been investigated and proven effective in terms of system stability, robustness and large-signal dynamics [4], [7]–[9].

Sliding-mode control (SMC) is an attractive nonlinear control method well-known for its intrinsic stability, robustness against parameter variations and simple implementation [8], [9]. Derived from the variable structure system theory [10], SMC extends the properties of hysteresis control into a multivariable system [11]. Much like a hysteresis controller, a SM controller alters the system structure to force the system states to "slide" along a predefined trajectory toward the desired equilibrium point. The control action of SMC is discontinuous and can be a simple on/off, making it particularly suitable for controlling switched-mode power supplies in which the circuit

alters its structure according to the status of the power switches. SM-controlled DC–DC converters have been shown to achieve excellent dynamic response over a wide range of operating conditions [8], [9]. A properly-implemented SM-controlled boost converter is able to achieve very fast dynamic response while guaranteeing large-signal stability [12].

1.4 Literature Review

Due to its desirable characteristics, SMC is a viable and promising approach to overcome the challenges in designing a fast and stable controller for the bus-forming boost converter. Focusing on the two challenges identified in Section 1.2, this section first reviews some of the important literatures on the conventional SMC design and points out a few drawbacks with the conventional approaches. Then, research publications focused on SM-controlled boost converters driving CPL are reviewed. Different methods for analyzing and controlling the highly nonlinear system are surveyed, revealing some areas that warrant further research.

1.4.1 Conventional SMC for Boost Converters

SMC for DC-DC converters has been investigated over the years [8], [9] and is still gaining momentum in the research community [12]–[17]. Implementations of SMC for DC–DC converters can be generally divided into two forms — direct and indirect. In the direct form, the discontinuous control law is directly implemented to produce the gate signal, which makes the design and implementation quite straightforward. In the indirect form, the SM control law is first translated to a continuous equivalent control signal [9] which is then passed through a pulse-width-modulation (PWM) unit for gate signal generation. Most of the research on SM-controlled DC-DC converters has been done in the indirect form partly due to the necessity of fixed-frequency

operation. However, implementation in the indirect form often involves a full set of state variables, and particularly for boost converters, it usually requires sensing the input and output voltages plus the inductor current and the output capacitor current [12], [13], resulting in increased cost and circuit complexity.

In theory, SM controllers are variable-frequency controllers. The variable switching frequency is not desirable with physical devices and complicates filter design. Therefore, for the direct form to be practical, the operating frequency has to be restricted or preferably fixed. The general-purpose SM controller presented in [8] and [11] can be considered as a direct form as there is no translation to an equivalent control signal, making it straightforward for implementation. The general-purpose SM controller can also achieve constant-frequency operation by the use of a ramp signal. The constant switching frequency coupled with the fact that only the output voltage and inductor current are needed to be sensed makes the general-purpose SM controller very attractive for controlling boost converters.

However, as discussed in [11], the general-purpose SM controller for boost converters, despite its simplicity in design and implementation, faces a major drawback as its dynamic performance is hindered by the use of a low-pass filter (LPF) for obtaining its inductor current reference.

1.4.2 SMC of Boost Converters with CPL

Traditional design and analysis of SM-controlled DC–DC converters have been mostly carried out with simple resistive loads [8], [9], [18]. However, in practical DC systems such as Figure 1.1, the loads are rarely purely resistive and often include CPLs. Considering the desirable

properties of SMC, there has been a growing interest in research focused on SM-controlled boost converters with CPLs [19]–[22].

In [19], a nonlinear sliding surface based on "power error" is proposed for boost converters supplying a CPL. In [20], the cascade connection of a SM-controlled boost converter feeding a SM-controlled buck converter acting as a CPL is studied. In these literatures, the load under study is pure CPL, whereas in real systems, the load often comprises a mix of CILs and CPLs. Such a mixed-load system has been considered in [21], where the authors proposed a SM controller based on a washout filter for bidirectional boost converters. In [22], a reduced-order model for the interleaved boost converter feeding resistive load and CPL is derived and verified in the small-signal sense to aid the design of a nonlinear-disturbance-observer-based SM controller.

From these recent publications, some areas for further research are identified. First, the basic SMC framework presented in [8] (i.e., the general-purposed SM controller) is still very viable for mixed-load systems, as demonstrated in [20] with a boost converter feeding only CPL; yet, this basic framework has not been extended to boost converters feeding both CIL and CPL, and there seems to lack a systematic approach (similar to the approach in [11]) to analyzing the dynamics and stability of the nonlinear system. Second, system dynamics have been studied primarily through phase-plane analysis [20], [21]; a closed-loop small-signal model for SM-controlled boost converters with mixed CIL and CPL has never been derived (perhaps due to the extreme nonlinearities in the system, as in this case, the converter, controller, and load are all nonlinear). However, a small-signal model would prove valuable in studying system dynamics and stability around the equilibrium point, and can lead to useful system transfer functions. Lastly, the SMC framework used in [20] for the CPL-only case requires prior knowledge of the load value that is

not easily accessible in practice; therefore, some form of load estimation is needed for this framework to be effective, if it were to be extended to the mixed-load case as well.

1.5 Research Objectives and Organization

This research focuses on the analysis, development, and implementation of SMC for boost converters with CIL and CPL. It aims to improve upon the existing state-of-the-art while presenting a systematic approach to analyzing systems dynamics and stability. New control strategies are proposed to enable better performance and stability. The research objectives and the layout of this thesis are as follows.

Objective 1: To improve upon the general-purpose SM controller for boost converters with CIL using observer-based approach

The general-purpose SM controller for boost converters [11] uses an LPF to obtain the inductor current reference. The LPF is required as a mean for automatic reference following, because for output voltage regulation of the boost converter, the inductor current reference value depends on the input voltage and load value, both of which are subject to variations. However, under line and/or load transients, the LPF causes delay for the inductor current reference signal to converge to the new target value. This inevitably degrades the dynamic performance of the system. To mitigate this problem, the Objective 1 is to propose an alternative approach to eliminate the LPF and establish the inductor current reference instantaneously. A state observer shall be employed to estimate the inductor current as feedback to the SM controller, reducing the number of costly current sensors used. Objective 1 is covered in Chapter 2.

Objective 2: To analyze the dynamics and stability of SM-controlled boost converters supplying both CIL and CPL

The second objective is to extend the basic SMC framework to boost converters supplying a mixed load comprising both CIL and CPL. The feasibility of the approach shall be studied systematically, where necessary conditions for stable SM operation shall be examined, and system dynamics shall be studied through the development of an accurate closed-loop small-signal model. Objective 2 is covered in Chapter 3.

Objective 3: To propose an adaptive SM controller for boost converters supplying mixed loads for improved performance and stability

The analysis from Objective 2 yields new insight into the dynamics and stability of the SM-controlled mixed-load system. Therefore, Objective 3 is to propose a new adaptive SM controller based on the newfound stability criterion to achieve improved dynamic response and guaranteed stability. A simple, practical load estimation technique shall be developed to supplement the proposed adaptive control. Objective 3 is covered in Chapter 4.

Chapter 2: The General-Purpose and Observer-Based Sliding-Mode Controllers for Boost Converters with Constant Impedance Load

In this chapter, the general-purpose SM controller [8] for CCM boost converters with CIL is first reviewed. The basic parameters and necessary conditions along with the theory of fixed-frequency operation are explained first, in order to set the stage for the development of a new observer-based fixed-frequency SM controller. Simulation studies are carried out at the end to verify the improved dynamic response of the proposed observer-based controller against the general-purpose controller for line and load transients.

2.1 The General-Purpose SM Controller for Boost Converters

The general-purpose SM controller [8] for the boost converter operating in CCM is illustrated in Figure 2.1. To simplify the system and focus only on the core concepts, parasitic elements are not included. The basic parameters and necessary conditions for stable SM operation are discussed in this section.

2.1.1 Controller Parameters

For the general-purpose SM controller depicted in Figure 2.1, the inductor current error and the output voltage error are chosen as the state variables as follows

$$x := \begin{cases} x_1 = i_L - i_{L\_ref} \\ x_2 = v_C - v_{C\_ref} \end{cases}, \tag{2.1}$$

where i_L and v_C are the inductor current and the capacitor voltage respectively, with i_{L_ref} and

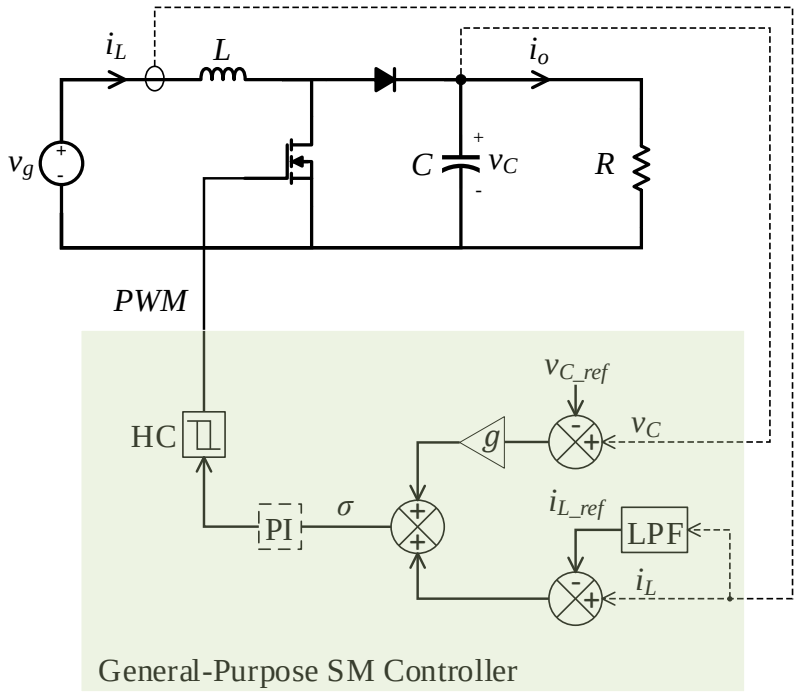

Figure 2.1 Schematic of the general-purpose SM controller for boost converters.

v_{C_ref} being their respective reference values.

The sliding function (σ) is a linear combination of the state variables, expressed as

$$\sigma = x_1 + gx_2 \,, \tag{2.2}$$

where g is a positive value known as the sliding coefficient that adjusts the response speed of the controller. The control law is thereby defined as

$$u = \begin{cases} 0 & for\ \sigma > 0 \\ 1 & for\ \sigma < 0 \end{cases}, \tag{2.3}$$

where u represents the switch status (0=OFF, 1=ON). The control law (2.3) is realized by a hysteresis controller (HC) to keep the sliding function (state trajectory) close to 0, resulting in the following sliding trajectory:

$$\sigma = x_1 + gx_2 = 0 \,. \tag{2.4}$$

A few remarks on the general-purpose SM controller in Figure 2.1 are made as follows. First, while v_{C_ref} is the desired output voltage, the inductor current reference i_{L_ref} is established by low-passing the inductor current i_L. In this case, a simple first-order LPF is used, where the transfer function for deriving the inductor current reference can be expressed as

$$H(s) = \frac{i_{L\_ref}(s)}{i_L(s)} = \frac{1}{\tau s + 1}, \tag{2.5}$$

where τ is the time constant of the LPF. According to [18], i_{L_ref} is considered an internal state variable reference which has its own dynamics due to its dependency on i_L.

Second, as shown in Figure 2.1, a proportional-integral (PI) controller is placed at the output of the system sliding function. The PI block is required to remove any steady-state error. This is known as integral SM control [13]. The PI block should only be activated once the system is operating on the sliding trajectory in order to preserve the large-signal dynamics of SMC [11]. Because of this and the relatively slow nature of the PI action, it is fair to exclude the PI controller from all the dynamic analysis.

Finally, the switching frequency of the SM controller depends on the rate of change of the system trajectory and the amplitude of the hysteresis band [8]. Therefore, to achieve fixed-frequency operation, the general-purpose SM controller uses a ramp signal injection onto the system trajectory (as shown in Figure 2.2). The theory of operation will be explained in a later section.

2.1.2 Necessary Conditions for Stable SM Operation

Generally speaking, the necessary conditions for stable SM operation are hitting, existence and stability conditions [11]. This section examines each of these terms and discusses the stability constraint with respect to the two critical parameters, g and τ.

2.1.2.1 Hitting Condition

The hitting condition is one of the necessary conditions for SM motion to happen. The hitting condition requires that the system's steady-state point for one substructure ends up in the phase region of the other substructure [11]. This guarantees that from any initial point, the state trajectory will eventually reach the sliding trajectory. The steady-state points of the boost converter system in Figure 2.1 for the two switch states are found to be

$$\begin{cases} i_L = \dfrac{v_g}{R}, & v_C = v_g, \quad i_{L\_ref} = i_L & for\ u = 0\ or\ \sigma > 0 \\ i_L = \infty, & v_C = 0, \quad i_{L\_ref} = I_{L\_ref\_sat} & for\ u = 1\ or\ \sigma < 0 \end{cases}, \tag{2.6}$$

where $I_{L\_ref\_sat}$ is the maximum inductor current reference value (as realistically the output of the LPF should be saturated at some finite upper limit imposed by the designer). By substituting the steady-state values in (2.6) into (2.2), it can be shown that the system's steady-state representative point (Σ) of one switch state falls within the phase region reserved for the other switch state, such that

$$\begin{cases} \Sigma_{u=0,\sigma>0} \in \sigma < 0 \\ \Sigma_{u=1,\sigma<0} \in \sigma > 0 \end{cases}, \tag{2.7}$$

hence satisfying the hitting condition.

2.1.2.2 Existence Condition

The existence condition ensures that the state trajectory is always directed toward the sliding trajectory in a small region close to the sliding trajectory [11] (so the state trajectory does not diverge). This is akin to the concept of asymptotic stability of the equilibrium point in modern control theory. The existence condition can be formulated as [11]

$$\lim_{\sigma\to 0^+} \dot{\sigma} < 0 \quad \text{and} \quad \lim_{\sigma\to 0^-} \dot{\sigma} > 0\,, \tag{2.8}$$

where $\dot{\sigma}$ denotes the time derivative of the sliding function (2.2).

To enforce (2.8) around the equilibrium point, the dynamic equations of the boost converter in CCM with CIL, including the dynamics of the inductor current reference (2.5), during switch ON and OFF are first derived as follows. Note that since we are analyzing in a small region around an operating point, v_g is replaced by its DC value V_g and the load R is considered non-changing.

$$\begin{cases} \dot{i}_L = \dfrac{1}{L}\left(V_g - v_C\right), \quad \dot{v}_C = \dfrac{1}{C}\left(i_L - \dfrac{v_C}{R}\right) & for\ u = 0 \\ \dot{i}_L = \dfrac{1}{L}V_g, \quad \dot{v}_C = \dfrac{1}{C}\left(-\dfrac{v_C}{R}\right) & for\ u = 1 \\ \dot{i}_{L\_ref} = -\dfrac{1}{\tau}i_{L\_ref} + \dfrac{1}{\tau}i_L & for\ both\ u = 0\ and\ 1. \end{cases} \tag{2.9}$$

in which $\dot{i}_L$ denotes the time derivative of i_L and so on. Next, the derivative of the sliding function (2.2) is written as

$$\dot{\sigma} = \dot{i}_L - \dot{i}_{L\_ref} + g\,\dot{v}_C\,. \tag{2.10}$$

Substituting (2.9) into (2.10) and evaluating using the steady-state equilibrium values, it can be shown that both of the inequality constraints in (2.8) lead to the following condition

$$g < \frac{RC}{L}\frac{V_g}{V_c} \quad \text{or} \quad g < \frac{RCD'}{L}\,, \tag{2.11}$$

where V_c is the steady-state capacitor voltage ($V_c = v_{C\_ref}$) and D is the steady-state duty cycle with $D' = 1 - D = V_g/V_C$.

It is important to note that the existence condition (2.8) is being evaluated at the equilibrium point which assumes the filtered inductor current reference signal has already converged to the steady-state value. As a result, the existence analysis does not yield information about the selection of the time constant τ for the LPF. To find the permissible range of τ, we have to examine the system dynamics through small-signal modeling [11].

2.1.2.3 Small-Signal Modeling and Stability around Equilibrium

The general methodology for deriving closed-loop small-signal models for converters under SMC has been discussed in [18]. A closed-loop small-signal model for the SM-controlled boost converter with CIL (as in Figure 2.1) has been derived in [11]. Therefore, this section will only report the stability results relevant to our analysis at hand.

Based on the closed-loop small-signal model in [11], we can use linear technique such as eigenvalue analysis or Routh–Hurwitz theorem to find the stability limit around the equilibrium point. The stability limit for the sliding coefficient g is found to be the same as in (2.11), and the stability limit for τ is found to be

$$\tau > \frac{Lg}{D'(RD'g + 2)}. \tag{2.12}$$

It is noted that, in addition to satisfying the constraint in (2.12), the choice of τ affects the system performance in terms of speed and damping of the response [8]. Therefore, both g and τ need to be tuned to meet the dynamic requirements of the system.

2.1.3 Fixed-Frequency Operation

For practical reasons, it is desirable to have the SM-controlled system operate at a constant frequency. In the general-purposed SM controller [11], a simple frequency-limiting technique has been presented where a ramp signal (w) is added on to the system trajectory (σ_e), as illustrated in Figure 2.2. The modified system trajectory (σ_f) is subjected to the control law (2.3) adapted to a hysteresis band (ΔB) as

$$u = \begin{cases} 0 & for\ \sigma_f > \Delta B/2 \\ 1 & for\ \sigma_f < -\Delta B/2 \end{cases}. \tag{2.13}$$

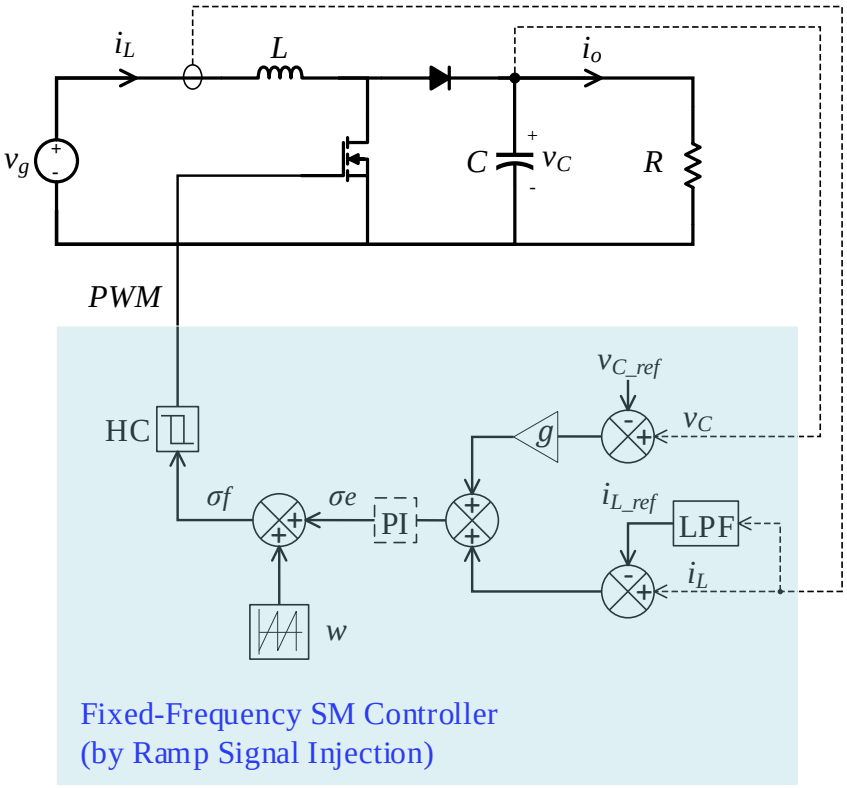

Figure 2.2 Schematic of the general-purpose SM controller for boost converters with fixed-frequency operation using ramp signal injection.

To illustrate the point of our discussion, Figure 2.3 shows (a) the system trajectory, (b) the injected ramp signal, (c) the modulated system trajectory and (d) the generated PWM signal, while the system is operating under sliding regime. As shown in Figure 2.3, the switching frequency is fixed to the frequency of the ramp signal and the hysteresis band functions to guarantee a minimum turn-on and turn-off time.

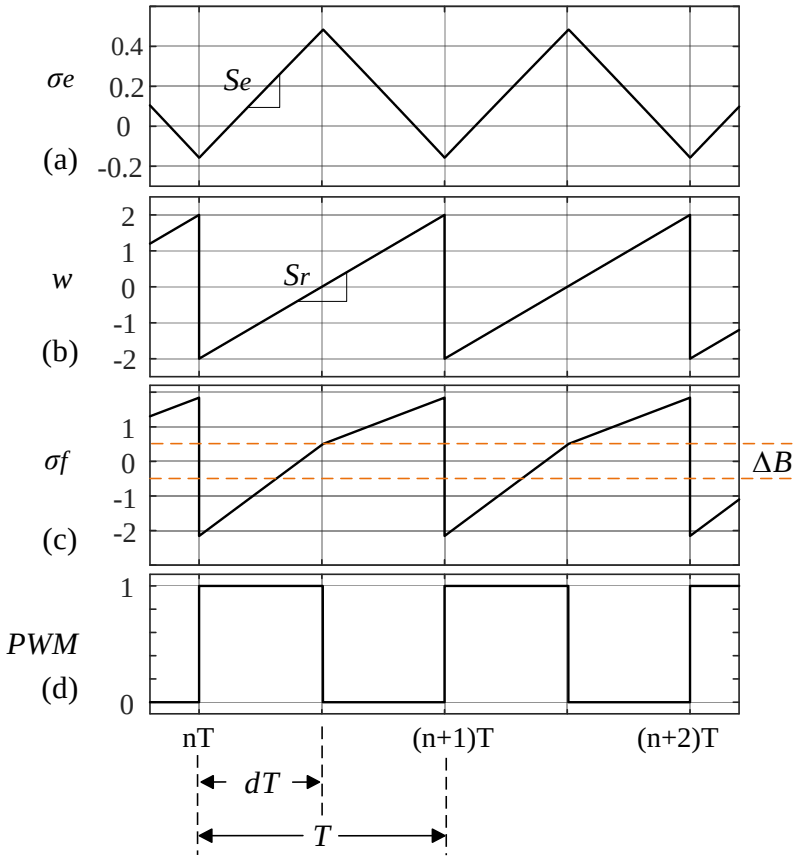

Figure 2.3 The internal parameters of the general-purpose SM controller while operating with fixed frequency using ramp signal injection.

In Figure 2.3, S_e and S_r are the rising slopes of the system trajectory and the ramp signal respectively. For stable constant-frequency operation, as inferred from Figure 2.3, they must satisfy the following condition [11]

$$S_e + S_r > \frac{\Delta B}{dT}. \tag{2.14}$$

2.2 Observer-Based Fixed-Frequency SM Controller

Passing the inductor current through an LPF to obtain its reference signal inevitably compromises the dynamic performance of the SM-controlled system. This section presents an alternative observer-based approach in which the inductor current reference is computed instantaneously by monitoring the input voltage and output current. To minimize the number of sensors used, a state observer based on the Kalman filter is used to estimate the inductor current as feedback to the SM controller.

2.2.1 Inductor Current Reference and Stability

Since the load under study is CIL, the equivalent load resistance value R can be easily computed using the measured output voltage v_c and output current i_o as

$$R = \frac{v_c}{i_o}. \tag{2.15}$$

The inductor current reference i_{L_ref}, which is also the steady-state inductor current, can be derived from the converter's behavioral model as

$$i_{L\_ref} = \frac{v_{C\_ref}}{RD'} = \frac{{v_{C\_ref}}^2}{Rv_g}. \tag{2.16}$$

Following the analysis in [11], it can be shown that the existence and stability conditions are now governed by (2.11) only, due to the removal of the LPF.

However, it is noted that the proposed way of establishing the inductor current reference requires monitoring the input voltage and output current in addition to the measurements required by the general-purpose SM controller. To reduce cost, the inductor current sensor can be eliminated by using a state observer, which will be developed in the following sections.

2.2.2 Duty Cycle Synthesis

To construct a state observer, the control signal, i.e., the duty cycle, must be known. In the indirect form of implementing SM control, the main method for obtaining the duty cycle is through the equivalent control approach by assuming the invariance conditions ($\sigma = 0$ and $\dot{\sigma} = 0$) during SM operation [13]. For implementation in the direct form, such as the general-purpose SM controller in Figure 2.2, a method to synthesize the duty cycle is developed here.

It is instructive to analyze the signals in Figure 2.3, without the hysteresis band ($\Delta B = 0$), as depicted in Figure 2.4. Let T denote the switching period and d denote the duty cycle for a particular switching cycle. For the following analysis, the beginning of a switching cycle commences at the falling edge of the ramp signal, as in Figure 2.4. The overbar ($\bar{}$) denotes a signal value sampled at the beginning of a switching cycle. Based on the converter's behavioral model, the rising slope of the system trajectory during dT (switch ON) is expressed as

$$S_e = \frac{di_L}{dt} + g\frac{dv_c}{dt} = \frac{\overline{v_g}}{L} + g\frac{-\overline{v_c}}{RC}. \tag{2.17}$$

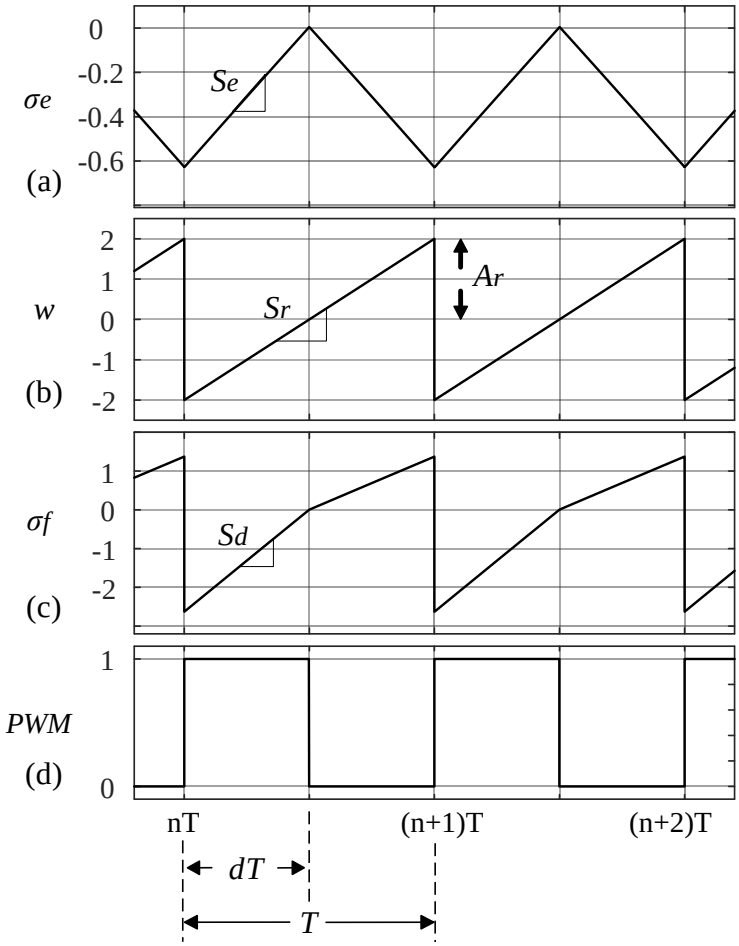

Figure 2.4 The internal parameters of the SM controller while operating with fixed frequency using ramp signal injection without hysteresis band.

Let A_r denote the peak amplitude of the injected ramp signal as shown in Figure 2.4, then the slope of the ramp signal is

$$S_r = \frac{2A_r}{T}. \tag{2.18}$$

The combined rising slope or the slope of σ_f during dT is

$$S_d = S_e + S_r. \tag{2.19}$$

Let σ_{e0} denote the system trajectory point sampled at the beginning of the switching cycle; according to (2.1) and (2.2), σ_{e0} can be computed as

$$\sigma_{e0} = \left(\overline{i_L} - i_{L\_ref}\right) + g\left(\overline{v_c} - v_{C\_ref}\right). \tag{2.20}$$

Then the duty ratio d_s for a particular switching period when the system is operating on the sliding trajectory can be formulated as

$$d_s = \frac{|\sigma_{e0} - A_r|}{TS_d}. \tag{2.21}$$

The result in (2.21) projects the duty ratio for a switching cycle at its start and is applicable when the system is operating on the sliding trajectory. To find the duty cycle everywhere, including when the system is operating in the reaching phase, the lower and upper values of the modified system trajectory are defined as

$$\begin{matrix} \sigma_{LOW} = \sigma_{e0} - A_r \\ \sigma_{HIGH} = \sigma_{e0} + TS_d \end{matrix}; \tag{2.22}$$

the duty cycle based on the fixed-frequency operation can then be formulated as

$$d = \begin{cases} 0, & \sigma_{LOW} > 0 \\ d_s, & \sigma_{LOW} < 0 \; and \; \sigma_{HIGH} > 0 \\ D_{max}, & \sigma_{HIGH} < 0 \end{cases}, \tag{2.23}$$

where D_{max} represents the maximum duty cycle limit.

The proposed fixed-frequency SM controller with the duty cycle synthesis function can be implemented in one digital block as depicted in Figure 2.5. A clock pulse at the switching frequency is used for sampling trigger. The ramp signal and the hysteresis block are both replaced by the adjustable parameters A_r and D_{max}. Using a sample-and-hold unit, a continuous duty cycle signal is produced based on (2.17)–(2.23).

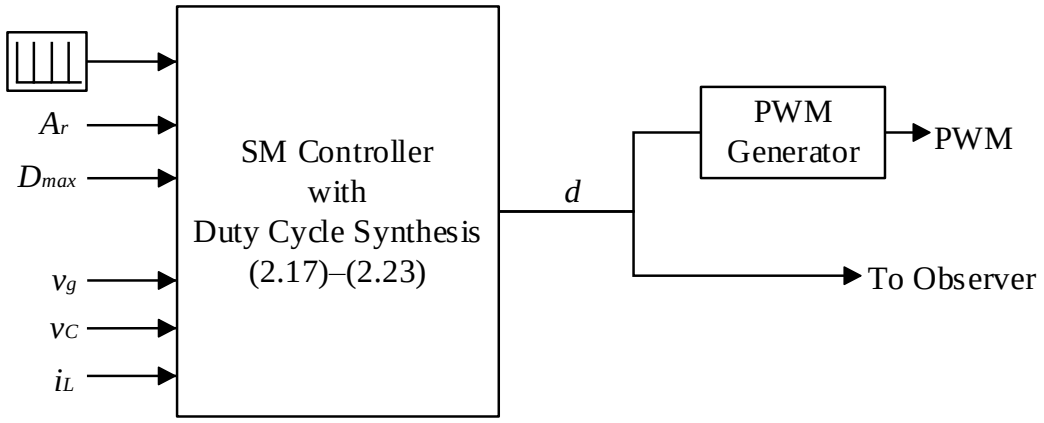

Figure 2.5 Implementation of the proposed fixed-frequency SM controller with duty cycle synthesis.

2.2.3 Observer Design

With the duty cycle known, the averaged model for CCM boost converter is used to construct a state observer to estimate the inductor current. Considering that the proposed SM controller will be implemented in a digital environment, the discretized state-space behavioral model of the system is first derived as

$$x[k+1] = \underbrace{\begin{bmatrix} 1 & -\frac{Td'[k]}{L} \\ \frac{Td'[k]}{C} & 1-\frac{T}{RC} \end{bmatrix}}_{A[k]} x[k] + \underbrace{\begin{bmatrix} \frac{T}{L} \\ \frac{T^2 d'[k]}{2LC} \end{bmatrix}}_{B[k]} v_g[k] \tag{2.24}$$

$$z[k] = \underbrace{[0 \quad 1]}_{H} x[k]$$

where the input voltage $v_g[k]$ is taken as the model input, $x[k] = [i_L[k], v_c[k]]^T$ are the state variables, $d[k]$ is the duty cycle where $d'[k] = 1 - d[k]$, T is the discretization time step, R is the load value given by (2.15), and $z[k]$ is the system output.

The state matrix $A[k]$ in (2.24) is time-varying but deterministic as the time-varying parameters R and $d[k]$ can be readily obtained using (2.15) and (2.23) at any step. This essentially

turns into an estimation problem for a linear time-varying system, for which the Kalman filter is the optimal filter/state estimator [23]. The readers are referred to [24] for an overview of the Kalman filter and its industrial applications. One way of implementing the recursive Kalman filter algorithm is illustrated in Figure 2.6, which can be directly applied to the considered system represented by (2.24).

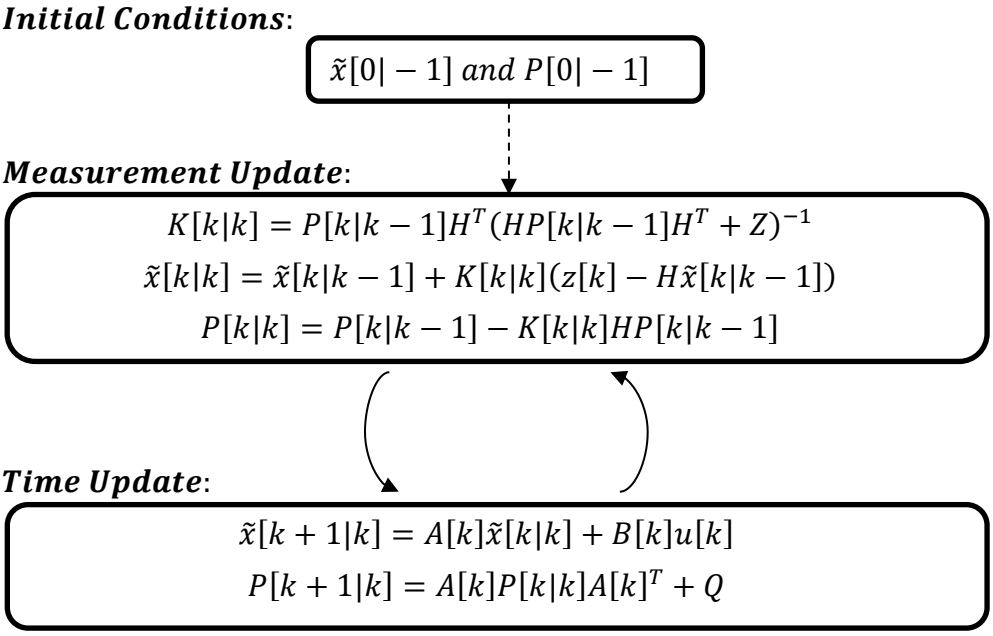

Figure 2.6 Implementation of the Kalman filter.

In the implementation of Kalman filter depicted in Figure 2.6, $\tilde{x}$ is the estimated state, P is the error covariance, u is the model input, z is the measurement, Q and Z are the covariances of the process and measurement noises which shall be white Gaussian noises uncorrelated to each other. However, noises in DC-DC converters are not purely Gaussian white, and their covariance properties are not readily available. For simplicity and proof of concept, the noise terms, i.e., Q

and Z, as well as any stochastic parametric uncertainties, are not considered in the scope of this work. The overall schematic of the proposed fixed-frequency SM controller with duty synthesis and state observer is shown in Figure 2.7.

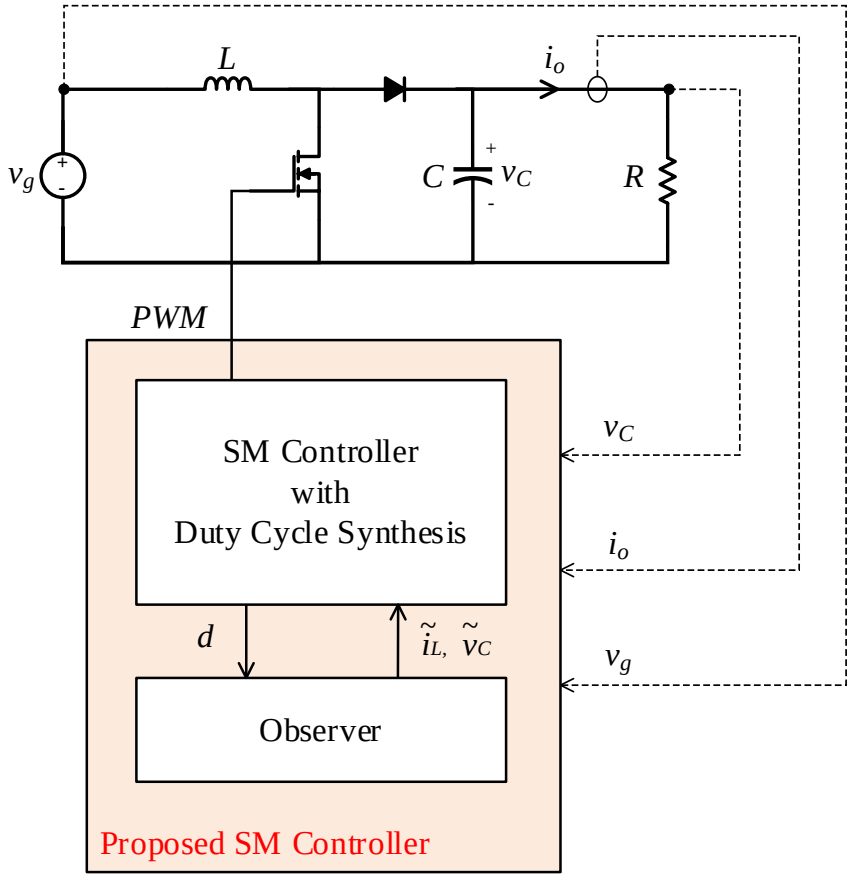

Figure 2.7 Implementation of the proposed observer-based fixed-frequency SM controller.

2.3 Simulation Studies

The performance of the proposed observer-based SM controller is investigated and compared with the general-purpose SM controller. The considered boost converter system with CIL is implemented in MATLAB/Simulink using both controllers with the parameters listed in Table 2.1.

Boost converter parameters:		
V_g = 24Vnominal	L = 0.15mH	A_r = 2V
V_o = 48V	C = 104uF	D_{max} = 0.99
I_o = 10Amax	f_{sw} = 100kHz	
Proposed SM Controller:	g = 0.07	
General SM Controller 1:	g = 0.07, τ = 1e-4	
General SM Controller 2:	g = 0.35, τ = 2e-4	

Table 2.1 System parameters for simulation studies

The sliding coefficient g of the proposed SM controller is first tuned to be 0.07. For comparison, the same g value is used for a general-purpose SM controller, with an appropriate τ (1e-4) chosen for the LPF based on (2.12). Then, a second general-purpose SM controller is tuned with best effort (g=0.35 and τ=2e-4) to optimize the system's start-up and transient response for a fair comparison. The dynamic performance of the three controllers is explored under various transients in the system.

Figure 2.8 shows the simulation results for the regulated output voltage of the boost converter under full load (4.8Ω) when the input voltage (v_g) experiences step changes. During the test scenario, v_g is stepped up from 24V to 36V at t=3ms, then stepped down to 24V at t=6ms, and

further stepped down to 20V at t=9ms. As it can be observed from Figure 2.8, the proposed controller demonstrates faster dynamic response with less over/undershoots against line disturbances compared with the general controller in both cases (with two sets of parameters).

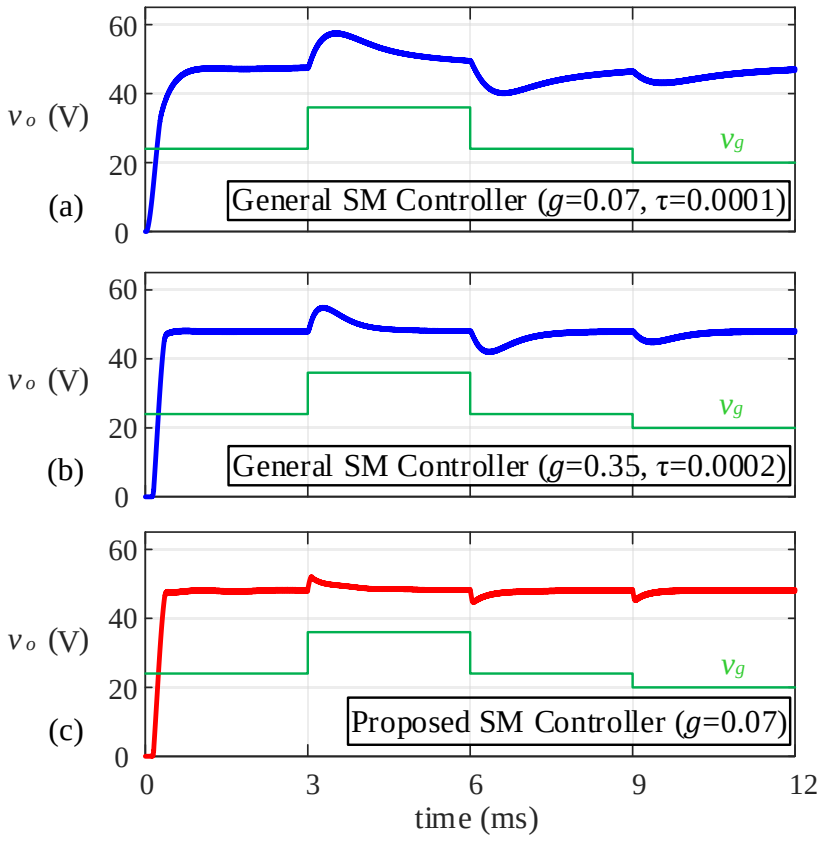

Figure 2.8 Output voltage regulation of the SM-controlled boost converter under full load condition against line disturbances using (a) the general SM controller, (b) the fine-tuned general SM controller, and (c) the proposed observer-based SM controller.

Figure 2.9 shows the simulation results for the regulated output voltage of the boost converter when the output load (denoted by its equivalent resistance R) experiences step changes. During the test scenario, the input voltage is kept constant at 24V, and R is stepped up to 9.6Ω (half-load) from 4.8Ω (full-load) at t=3ms and then stepped back to 4.8Ω at t=6ms. As it can be observed from Figure 2.9, the proposed controller shows superior performance in regulating the output voltage against load disturbances.

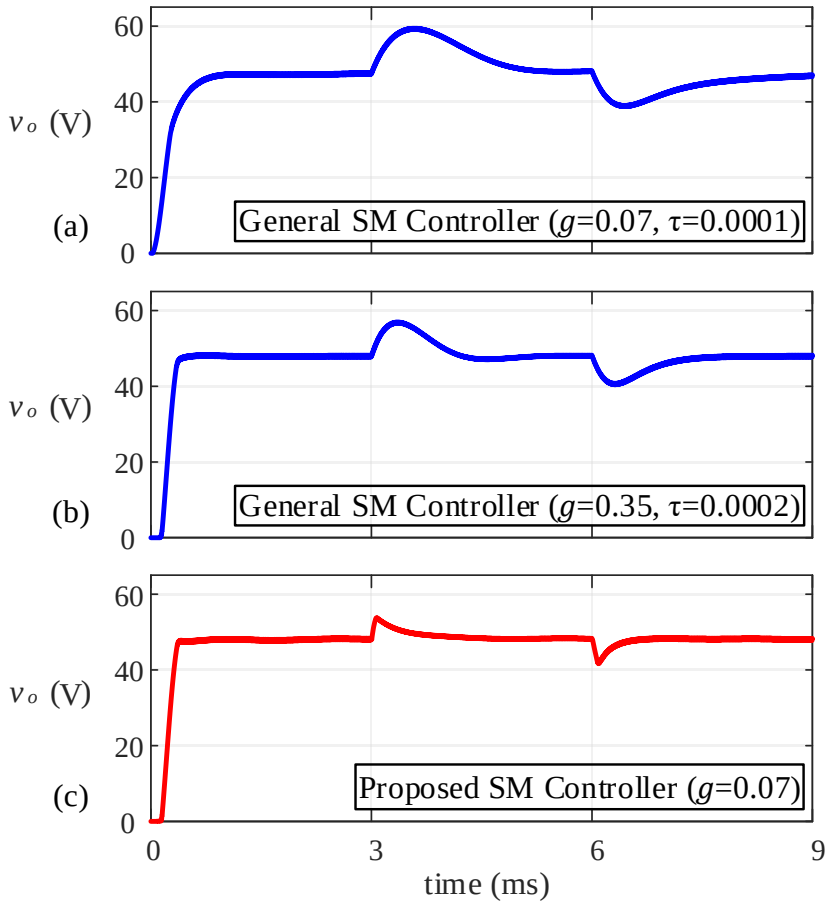

Figure 2.9 Output voltage regulation of the SM-controlled boost converter with constant input voltage against load disturbances using (a) the general SM controller, (b) the fine-tuned general SM controller, and (c) the proposed observer-based SM controller.

2.4 Summary

In this chapter, the basic sliding-mode control framework for DC–DC boost converters with constant impedance load is revisited. Controller parameters and stability conditions are explained in detail. A new observer-based fixed-frequency sliding-mode controller has been proposed. The proposed controller requires only one additional voltage sensor for the input voltage compared to the general-purpose sliding-mode controller, as the inductor current sensor is moved to the output with the use of an observer, thereby keeping cost low. The proposed controller eliminates the low-pass filter, resulting in a significant improvement in transient performance, as validated by various simulation studies. From efficiency and reliability standpoints, the improved dynamic performance with faster convergence speed and reduced over/undershoot will result in less energy loss during system transients and less stress on the components, leading to prolonged useful life.

Chapter 3: Analysis of Sliding-Mode-Controlled Boost Converters with Constant Impedance and Constant Power Loads

In this chapter, the basic SMC framework presented in the last chapter is extended to controlling boost converters supplying both CIL and CPL. The necessary conditions for stable SM operation are analyzed in a systematic manner. A closed-loop small-signal model for the SM-controlled mixed-load system is derived, leading to new insight into the dynamics and stability of the nonlinear system.

3.1 SMC of Boost Converters with Mixed Loads

The general-purpose SM controller for boost converters operating in CCM is again used as the basic framework here, as depicted in Figure 3.1. The load is represented by a resistive load (CIL) in parallel with an ideal CPL. The system state variables x, sliding function σ, control law u and the sliding trajectory are the same as they were defined in Section 2.1.1 (2.1)–(2.4).

However, the basic SMC framework must be modified in order to work with the mixed-load system. Specifically, the inductor current reference must be reformulated to account for the nonlinear CPL, and the necessary conditions for stable SM operation, i.e., the hitting, existence and stability conditions, must be examined and satisfied.

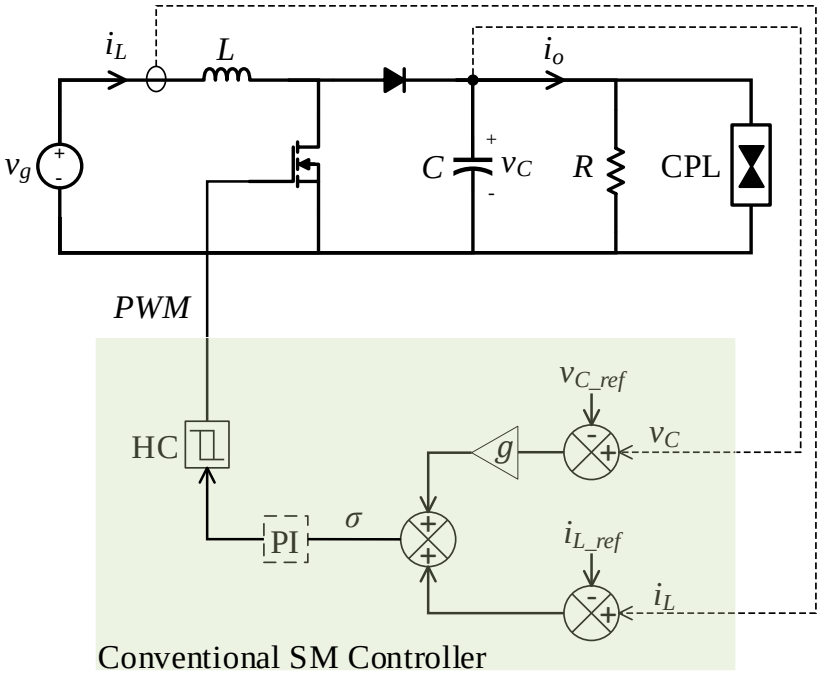

Figure 3.1 Schematic of the conventional SM controller for boost converters feeding both CIL and CPL.

3.1.1 Inductor Current Reference

In contrast to the simple CIL case, the formulation of the inductor current reference i_{L_ref} for the mixed-load system is rather complicated due to the presence of the CPL. Assuming the resistive load value (R) and the CPL power (P_{CPL}) are known, together with the input voltage (v_g), i_{L_ref} can be formulated as

$$i_{L\_ref} = \frac{{v_{C\_ref}}^2}{v_g R} + \frac{P_{CPL}}{v_g}. \tag{3.1}$$

In (3.1), the second part on the right side concerning P_{CPL} is formulated based on the adaptive law used in [20] which recognizes that the converter is a POPI (Power Out = Power In) network. However, one important assumption here is that the values of R and P_{CPL} are available. In real systems, loads are constantly changing and load values are unknown due to the fact that separating

and monitoring each and every load branch are impractical; the only load information available is likely the total output current (i_o) from the converter. Therefore, by lumping the CILs and CPLs together and utilizing the POPI concept, the control law for setting i_{L_ref} is adopted as follows,

$$i_{L\_ref} = \frac{P_{out}}{v_g} = \frac{v_C i_o}{v_g}, \tag{3.2}$$

in which v_C is the instantaneous output voltage of the converter instead of the static v_{C_ref} in (3.1) and $i_o = \frac{v_C}{R} + \frac{P_{CPL}}{v_C}$ (however R and P_{CPL} are unknown in this case). According to [18], i_{L_ref} defined in (3.2) is considered an internal state variable reference which has its own dynamics due to its dependency on v_C.

3.1.2 Hitting Condition

The concept of the hitting condition was explained in Section 2.1.2.1. To examine whether the conventional SM controller in Figure 3.1 with the adopted inductor current reference law (3.2) satisfies the hitting condition, the steady-state points of the mixed-load system for the two switch states are found,

$$\begin{cases} i_L = \frac{v_g}{R} + \frac{P_{CPL}}{v_g}, \;\; v_C = v_g, \;\; i_{L\_ref} = i_L & for\ u = 0\ or\ \sigma > 0 \\ i_L = \infty, \quad v_C = 0, \quad i_{L\_ref} = 0 & for\ u = 1\ or\ \sigma < 0 \end{cases}. \tag{3.3}$$

By substituting the steady-state values in (3.3) into the sliding function (2.2), it can be shown that the system's steady-state representative point of one switch state falls within the phase region reserved for the other switch state, hence satisfying the hitting condition (2.7).

3.1.3 Existence Condition and Internal Stability

The hitting condition guarantees that the state trajectory will reach the sliding trajectory from any initial condition. By solving for $\sigma = 0$ and $\dot{\sigma} = 0$, it can be easily shown that (x_1, x_2) = (i_{L_ref} [as defined in (3.2)], v_{C_ref}) is a unique equilibrium point. Therefore, we need to assess the condition for this equilibrium point to be asymptotically stable.

The definition of the existence condition was explained in Section 2.1.2.2. Before we assess the existence condition (2.8), it is instructive to point out its connection to Lyapunov's direct method. If we define a Lyapunov function (an "energy" function) as

$$V(\sigma) = \frac{1}{2}\sigma^2 , \tag{3.4}$$

the derivative of $V(\sigma)$ is

$$\dot{V} = \sigma\dot{\sigma} . \tag{3.5}$$

By Lyapunov's direct method for asymptotic stability, we force $\dot{V} < 0$ which leads to

$$\sigma\dot{\sigma} < 0 , \tag{3.6}$$

which can also be evaluated by the inequalities in (2.8).

To enforce (2.8) around the equilibrium point, the dynamic equations of the system in CCM, including the dynamics of the inductor current reference in (3.2), during switch ON and OFF are derived in (3.7) as follows. Since we are only interested in a small region around the steady-state operating point, v_g is replaced by its DC value V_g and the load values R and P_{CPL} are considered non-changing.

$$\begin{cases} \dot{i}_L = \frac{1}{L}(V_g - v_C), \dot{v}_C = \frac{1}{C}\left(i_L - \frac{v_C}{R} - \frac{P_{CPL}}{v_C}\right) & for\ u = 0 \\ \dot{i}_L = \frac{1}{L}V_g, \dot{v}_C = \frac{1}{C}\left(-\frac{v_C}{R} - \frac{P_{CPL}}{v_C}\right) & for\ u = 1 \\ \dot{i}_{L\_ref} = \frac{2}{R}\frac{v_c}{V_g}\dot{v}_C & for\ both\ u = 0\ and\ 1. \end{cases} \tag{3.7}$$

Next, the derivative of the sliding function (2.2) is written as

$$\dot{\sigma} = \dot{i}_L - \dot{i}_{L\_ref} + g\,\dot{v}_C\,. \tag{3.8}$$

Substituting (3.7) into (3.8) and evaluating using the equilibrium values, it can be shown that both of the inequality constraints in (2.8) lead to the following condition:

$$g < \frac{2}{RD'} + \frac{CD'}{L}\left(\frac{1}{R} + \frac{P_{CPL}}{{V_c}^2}\right)^{-1}. \tag{3.9}$$

Thereby, we can say that (3.9) satisfies Lyapunov's criterion for asymptotic stability at the equilibrium point, or in other words, (3.9) dictates the existence condition for a small region around the equilibrium point.

If the load is pure CPL, then the stability condition (3.9) reduces to

$$g < \frac{CV_gV_C}{LP_{CPL}} \quad \text{or} \quad P_{CPL} < \frac{CV_gV_C}{Lg}, \tag{3.10}$$

which agrees with the upper CPL power limit reported in [20].

This concludes a general analysis on the SM-controlled boost converter feeding both CIL and CPL. In the next section, we study the system dynamics around the equilibrium point using small-signal modeling.

3.2 Small-Signal Modeling of SM-Controlled Boost Converters with Mixed Loads

This section derives a closed-loop small-signal model for the SM-controlled mixed-load system. From the linearized model, system stability around equilibrium point is examined and system dynamics are studied through closed-loop transfer functions, which are compared with detailed circuit simulations.

3.2.1 Small-Signal Modeling of the Mixed-Load System under SMC

Following the general methodology in [18], the small-signal modeling of the SM-controlled boost converter system in Figure 3.1 begins with the average modeling of the system in open loop. Based on (3.7), the dynamic equations for the averaged model of the open-loop boost converter in CCM, including the dynamics of the inductor current reference, are first written as

$$\begin{cases} \dot{i}_L = \dfrac{1}{L}\left(v_g - d' v_C\right) \\ \dot{v}_C = \dfrac{1}{C}\left(d' i_L - \dfrac{v_C}{R} - \dfrac{P_{CPL}}{v_C} - \hat{i}_o\right) \\ \dot{i}_{L\_ref} = \dfrac{1}{v_g}\left(\dfrac{2}{R} v_C \dot{v}_C + v_C \dot{\hat{i}}_o + \hat{i}_o \dot{v}_C\right) \\ \qquad\qquad - \dfrac{1}{{v_g}^2}\left(\dfrac{{v_C}^2}{R} + P_{CPL} + v_C \hat{i}_o\right)\dot{v}_g \end{cases} . \tag{3.11}$$

Note that as we eventually linearize (3.11) by perturbation, we will introduce an output current perturbation ($\hat{i}_o$) leaving the converter's output node in parallel with the CIL and the CPL. If we perturb and linearize (3.11), i.e., $\hat{i}_o$ remains as is, $d' = (D' - \hat{d})$, $v_g = \left(V_g + \hat{v}_g\right)$, $v_C = (V_C + \hat{v}_C)$ and so on. Taking $\hat{v}_g$ and $\hat{i}_o$ as model inputs, we end up with input derivative terms $\dot{\hat{v}}_g$ and $\dot{\hat{i}}_o$, which are problematic when deriving system transfer functions later on. The approach proposed

here is to take the input derivative terms as additional model inputs and redefine the state vector $\hat{x}$ and input vector $\hat{u}$ as

$$\begin{aligned} \hat{x} &= \left[\hat{i}_L,\ \hat{v}_C,\ \hat{i}_{L\_ref}\right]^T \\ \hat{u} &= \left[\hat{v}_g,\ \dot{\hat{v}}_g,\ \hat{i}_o,\ \dot{\hat{i}}_o\right]^T . \end{aligned} \tag{3.12}$$

In this way, the linearized open-loop small-signal model can be written in standard state-space form as

$$\dot{\hat{x}} = A\hat{x} + B\hat{u} + E\hat{d}\ , \tag{3.13}$$

where

$$A = \begin{bmatrix} 0 & -\frac{D'}{L} & 0 \\ \frac{D'}{C} & \frac{1}{C}\left(\frac{P_{CPL}}{{V_c}^2} - \frac{1}{R}\right) & 0 \\ \frac{2}{CR} & \frac{2}{CRD'}\left(\frac{P_{CPL}}{{V_c}^2} - \frac{1}{R}\right) & 0 \end{bmatrix}, \tag{3.14}$$

$$B = \begin{bmatrix} \frac{1}{L} & 0 & 0 & 0 \\ 0 & 0 & \frac{1}{C} & 0 \\ 0 & -\frac{I_L}{V_g} & \frac{2}{CRD'} & -\frac{1}{D'} \end{bmatrix}, \tag{3.15}$$

$$E = \left[\frac{V_C}{L},\ -\frac{I_L}{C},\ -\frac{2I_L}{CRD'}\right]^T\ , \tag{3.16}$$

where $I_L = \frac{V_c}{D'}\left(\frac{1}{R} + \frac{P_{CPL}}{{V_C}^2}\right)$ is the steady-state inductor current.

Next, to derive the closed-loop small-signal model, we first describe the sliding function (2.2) in the small-signal sense in terms of the state variables defined in (3.12) as

$$\sigma = \hat{\imath}_L - \hat{\imath}_{L\_ref} + g\,\hat{v}_C = G\hat{x}\,, \tag{3.17}$$

where $G = [1, g, -1]$.

Then we apply the invariance condition for SMC [9], which assumes when the system is operating under sliding regime (i.e., at equilibrium),

$$\sigma = 0 \Longrightarrow \dot{\sigma} = 0 \Longrightarrow G\dot{\hat{x}} = 0\,. \tag{3.18}$$

Combining (3.13) and (3.18), $\hat{d}$ can be solved as

$$\hat{d} = (GE)^{-1}(-GA\hat{x} - GB\hat{u})\,. \tag{3.19}$$

$\hat{d}$ in (3.19) represents the duty cycle (control signal) perturbation when the system is operating under sliding regime with ideal sliding dynamics.

Finally, substituting $\hat{d}$ in (3.19) into (3.13), we arrive at the closed-loop small-signal model for the system under SMC:

$$\dot{\hat{x}} = (A - E(GE)^{-1}(GA))\,\hat{x} + (B - E(GE)^{-1}(GB))\,\hat{u}\,. \tag{3.20}$$

It can be noted that one of the states in (3.20) is redundant. Applying the invariance condition ($\sigma = 0$) again, we can substitute $\hat{\imath}_{L\_ref}$ with

$$\hat{\imath}_{L\_ref} = \hat{\imath}_L + g\,\hat{v}_C\,, \tag{3.21}$$

which reduces (3.20) to

$$\dot{\hat{x}}^* = A_T\hat{x}^* + B_T\hat{u}\,, \tag{3.22}$$

where $\hat{x}^* = \left[\,\hat{\imath}_L,\ \hat{v}_c\,\right]^T$ and A_T and B_T in closed form are

$$A_T = k\begin{bmatrix} D'(2 - D'Rg) & \dfrac{2D'Rg - 4}{R} \\ D'^2R & -2D' \end{bmatrix}, \tag{3.23}$$

$$B_T = k\begin{bmatrix} \frac{2 - D'Rg}{D'}Y & -\frac{CR}{D'}Y & 2 - D'Rg & -CR \\ RY & \frac{LR}{D'^2}Y^2 & D'R & \frac{LR}{D'}Y \end{bmatrix}, \tag{3.24}$$

where $k = \frac{1}{L\left(\frac{2}{D'} - Rg\right)Y + CD'R}$ and $Y = \frac{1}{R} + \frac{P_{CPL}}{{V_C}^2}$.

3.2.2 Remark on Stability Boundary at Equilibrium Point

If we test the stability of the linearized system (3.22)–(3.24) by eigenvalue analysis, we find that one eigenvalue of the state matrix A_T is zero and the other eigenvalue is

$$\lambda_{non-zero} = -\frac{D'^2 g}{LY\left(\frac{2}{RD'} + \frac{CD'}{L}Y^{-1} - g\right)}. \tag{3.25}$$

If we take g as the variable and force (3.25) to be negative (or its denominator to be positive), the resulting condition coincides with the existence condition (3.9). However, due to the zero eigenvalue, the asymptotic stability at the equilibrium point based on the linearized system is inconclusive; therefore, we have to rely on the existence condition (i.e., Lyapunov's direct method) for asymptotic stability of the equilibrium point.

Nonetheless, the stability analysis of the linearized system is not without merit. It is noted that the non-zero eigenvalue, if forced to negative, leads to the same condition as the existence condition. By Lyapunov's indirect method, if this non-zero eigenvalue is positive (i.e., if it violates the existence condition), then the equilibrium point of the nonlinear system is unstable. Therefore, we can infer that the existence condition (3.9) also constitutes the boundary for asymptotic stability of the equilibrium point of the nonlinear system. In the next chapter, we will use this stability boundary to design an adaptive SM controller.

3.2.3 Transfer Functions and Model Verification

From the developed small-signal model (3.22)–(3.24), useful transfer functions can be derived, such as input disturbance rejection (G_{vg}), also known as audiosusceptibility, and output impedance (Z_{out}). The subsystem transfer functions $G_{\hat{v}_g}(s)$, $G_{\dot{\hat{v}}_g}(s)$, $G_{\hat{i}_o}(s)$ and $G_{\dot{\hat{i}}_o}(s)$ defined as

$$\left.\begin{aligned} G_{\hat{v}_g}(s) &= \left.\frac{\hat{v}_c(s)}{\hat{v}_g(s)}\right|_{\dot{\hat{v}}_g=0,\hat{i}_o=0,\dot{\hat{i}}_o=0} \\ G_{\dot{\hat{v}}_g}(s) &= \left.\frac{\hat{v}_c(s)}{\dot{\hat{v}}_g(s)}\right|_{\hat{v}_g=0,\hat{i}_o=0,\dot{\hat{i}}_o=0} \end{aligned}\right\} G_{vg}(s) = G_{\hat{v}_g}(s) + sG_{\dot{\hat{v}}_g}(s)\,,$$

$$\left.\begin{aligned} G_{\hat{i}_o}(s) &= \left.\frac{\hat{v}_c(s)}{-\hat{i}_o(s)}\right|_{\dot{\hat{i}}_o=0,\hat{v}_g=0,\dot{\hat{v}}_g=0} \\ G_{\dot{\hat{i}}_o}(s) &= \left.\frac{\hat{v}_c(s)}{-\dot{\hat{i}}_o(s)}\right|_{\hat{i}_o=0,\hat{v}_g=0,\dot{\hat{v}}_g=0} \end{aligned}\right\} Z_{out} = G_{\hat{i}_o}(s) + sG_{\dot{\hat{i}}_o}(s)\,, \tag{3.26}$$

can be readily obtained using the general state-space-to-transfer-function formula:

$$G(s) = C_T(sI - A_T)^{-1}B_T\,. \tag{3.27}$$

where $C_T = [0, 1]$. The mathematical representation of the converter in small-signal domain is illustrated in Figure 3.2.

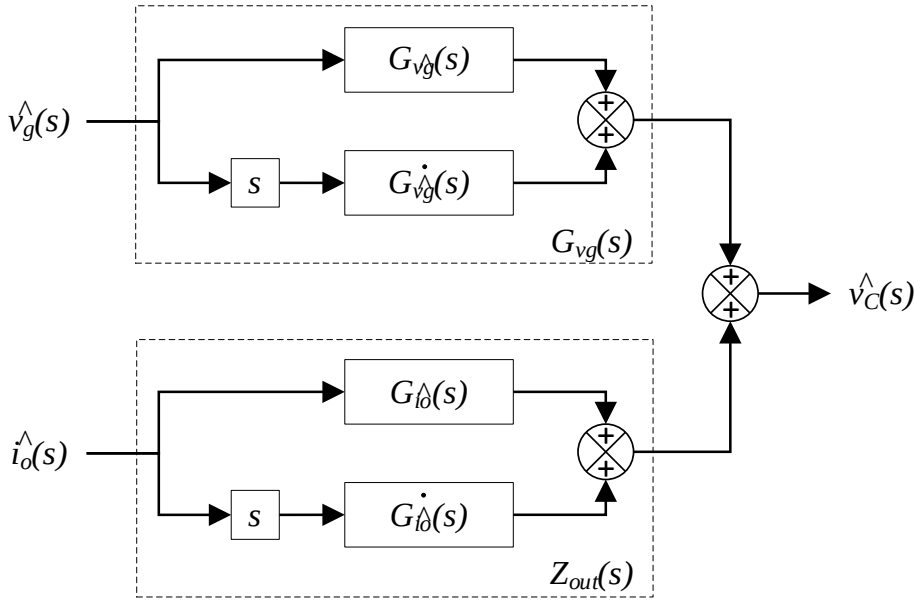

Figure 3.2 Transfer function representation of the small-signal converter model.

To validate the accuracy of the developed closed-loop small-signal model, an example SM-controlled boost converter system as shown in Figure 3.1 is considered. The converter parameters are specified in Table 3.1, with g=0.9, R=4.6Ω (500W) and P_{CPL}=1kW. The audiosusceptibility and output impedance of the system as predicted by the closed-loop small-signal model are compared with the frequency responses measured from switching circuit simulations in MATLAB/Simulink. The results are presented in Figure 3.3. As shown, the results predicted by the model (shown with solid lines) are in agreement with the circuit simulation results (shown with circles), which verifies the accuracy of the developed closed-loop small-signal model for SM-controlled boost converters with mixed loads.

V_g	V_c	L	C
24V	48V	3mH	1200uF

Table 3.1 Basic parameters of the example boost converter under study

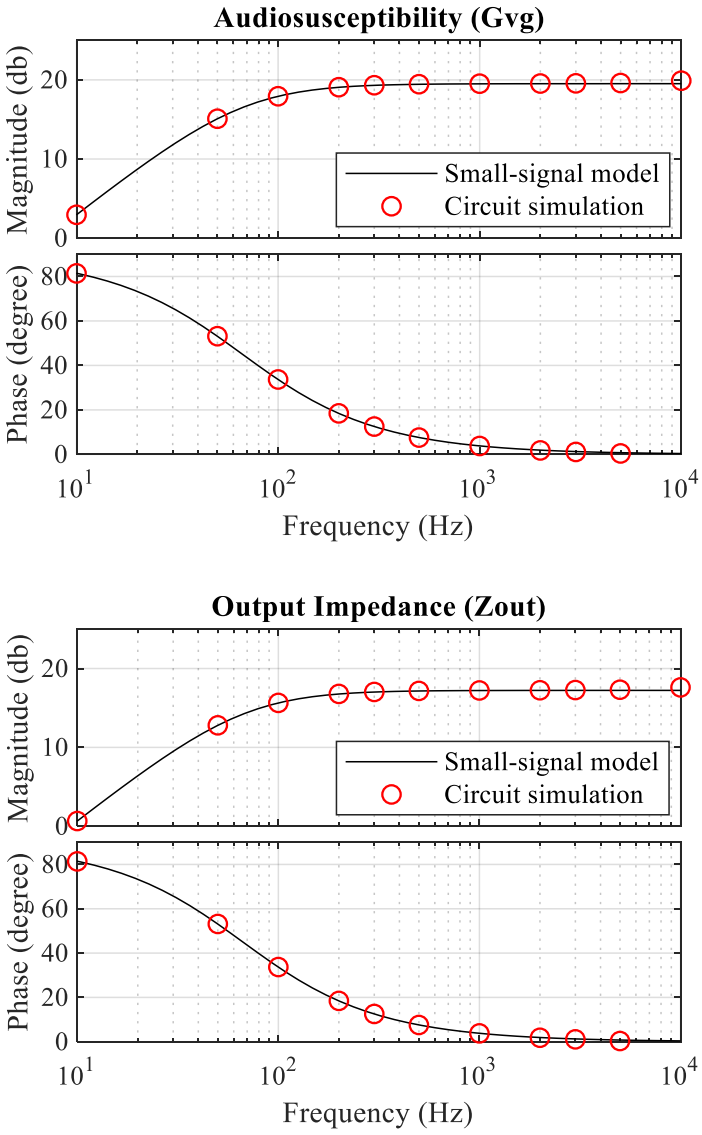

Figure 3.3 Audiosusceptibility and output impedance of the example boost converter system under SMC as obtained from the developed small-signal model and detailed circuit simulations (switching frequency≈50kHz).

3.3 Summary

In this chapter, the sliding-mode-controlled boost converter feeding constant impedance and constant power loads is analyzed. Necessary conditions for stable sliding-mode operation are examined rigorously, offering new perspectives on the existence/stability condition. System dynamics and stability are studied through the development of an accurate closed-loop small-signal model. From the analysis, system stability is characterized in terms of the sliding coefficient and load composition. The analytical approach presented in this chapter is sufficiently general and applicable to other converter topologies with mixed loads under sliding-mode control.

Chapter 4: Adaptive Sliding-Mode Control for Boost Converters with Mixed Loads

In the previous chapter, the stability condition for SM-controlled boost converters supplying mixed loads is established in terms of the sliding coefficient and load composition. By exploiting the newfound stability criterion, this chapter proposes a new adaptive SM controller featuring an adjustable sliding coefficient and a load estimation technique to achieve faster dynamic response and guaranteed stability. The theory of operation is explained in detail. Simulation studies and experimental validations using real-time simulator are included at the end to demonstrate the effectiveness of the proposed control.

4.1 Observations on the Stability Condition

It is instructive to rewrite the stability condition of (3.9) and express the maximum allowable g, i.e., g_{crit}, in terms of the resistive load power (P_R) and CPL power (P_{CPL}) as

$$g_{crit} = \frac{2P_R}{V_g V_c} + \frac{C}{L}\frac{V_g V_c}{P_R + P_{CPL}}. \tag{4.1}$$

To illustrate the implication of (4.1), the stability boundary in terms of g_{crit} and load compositions using the parameters in Table 3.1 is plotted in Figure 4.1.

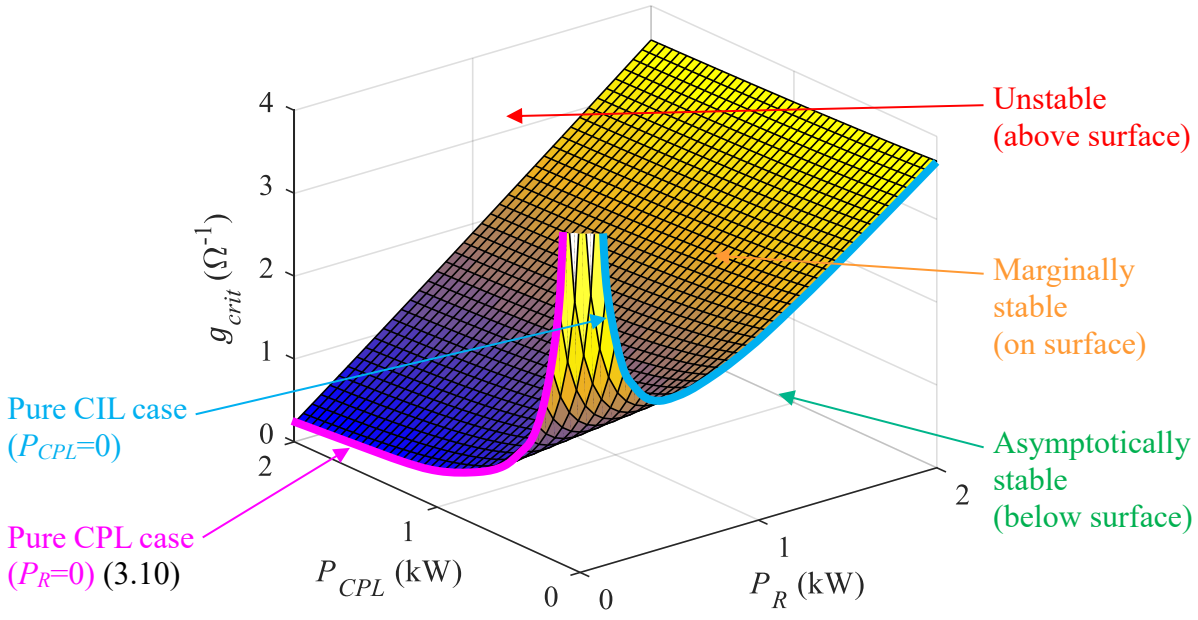

Figure 4.1 Stability boundary in terms of the maximum allowable g for the example boost converter system under SMC with different load compositions.

As observed in Figure 4.1, the stability condition when the load is pure CPL (3.10) corresponds to the "worst-case" line of the lowest g_{crit}, and g_{crit} increases as load shifts to be more resistive. Considering that the sliding coefficient g directly affects the convergence rate of the system, this means that tuning the controller based on (3.10) which only assumes CPL loading can become conservative when resistive load is present, and thus will not yield the best performance in a mixed-load environment.

4.2 Adaptive SMC with Adjustable Sliding Coefficient

To improve system performance, an adaptive SMC scheme with adjustable sliding coefficient g is proposed and depicted in Figure 4.2. In the proposed method, as opposed to the conventional SMC that adopts a static g, the stability condition (3.9) or (4.1) is used to continuously adjust g based on the load composition, so that the system operates just beneath the stability boundary (e.g., under the stability surface in Figure 4.1). This will ensure that a reasonably large g is selected (which yields fast response speed) while maintaining stability.

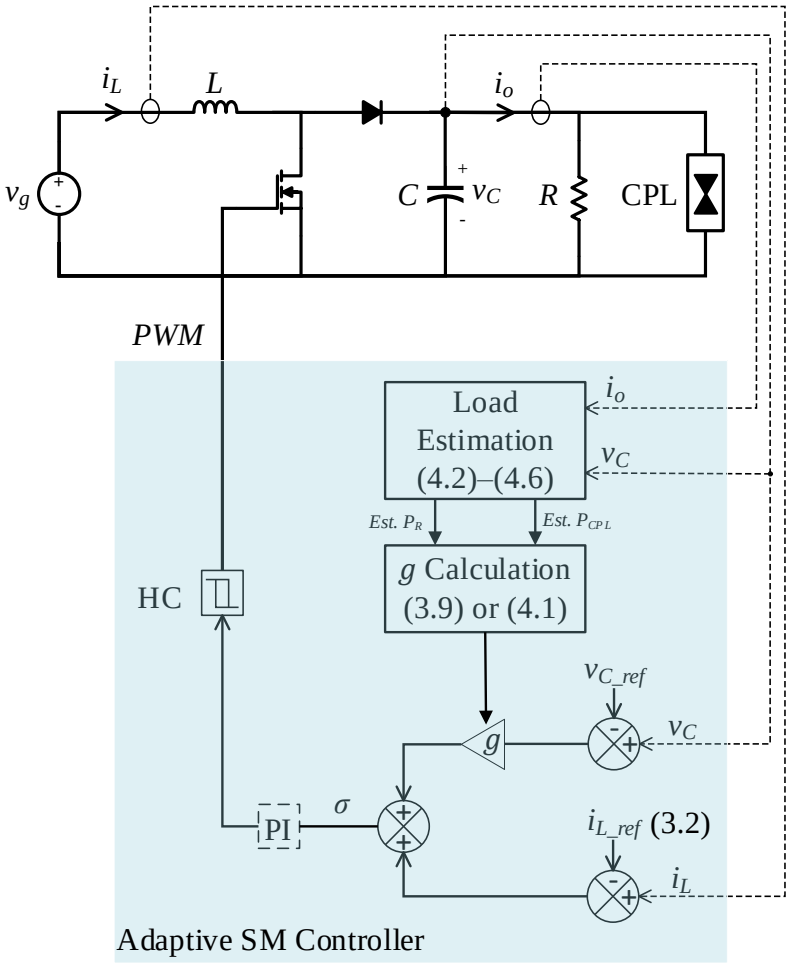

Figure 4.2 Schematic of the proposed adaptive SM controller with adjustable g and load estimation.

However, the proposed adaptive method requires knowledge of the instantaneous load composition, i.e., how much CIL and how much CPL are being supplied, as used in (4.1). In order to achieve this, conveniently, separate sensors can be deployed to monitor the currents through the CIL and CPL branches; however, this approach is costly and likely impractical [not to mention that it defeats the purpose of the inductor current reference law in (3.2)]. Considering this, a practical load estimation technique is proposed in the next section, which requires monitoring only the total output current from the converter and identifies the load composition based on the output switching ripples.

4.3 Load Estimation Using Switching Ripples

To illustrate the proposed load estimation technique, Figure 4.3 shows a simplified boost converter feeding a resistive load and an ideal CPL, along with steady-state waveforms of the output voltage, output currents and gate signal during CCM operation.

As shown in Figure 4.3 (b), during the interval $D'T$ when the switch is turned OFF, the output voltage v_o rises from v_1 to v_2; this causes the current through the resistive load to increase and the current through the CPL to decrease, as shown in Figure 4.3 (d). The combined output current profile i_o in Figure 4.3 (c) (whether it will increase or decrease and at what rate) will directly correspond to the ratio of resistive load to CPL. Therefore, assuming the loads are non-changing, theoretically, if we have two distinct sets of output voltage and current samples, then we can work out the load ratio/composition.

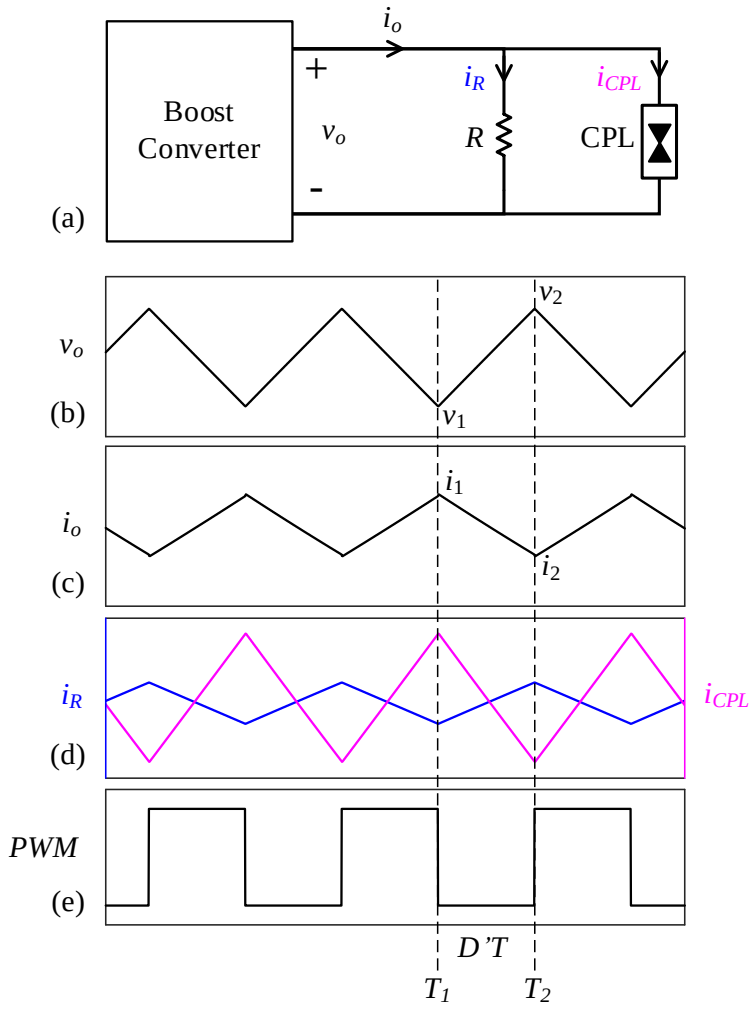

Figure 4.3 Steady-state waveforms of the boost converter in CCM: (a) simplified converter system emphasizing the load section, (b) output voltage, (c) output current, (d) currents through the two load branches, and (e) power switch gate signal.

The first voltage and current sampling can be triggered at either rising or falling edge of the gate signal, depending on the specific implementation. The second trigger point should be at the next switching action, since the magnitude difference between the two samples will be the largest, providing better resolution/accuracy, and also because load estimation should occur once

per switching cycle. In this example, we will use the falling edge as the first sampling trigger as shown in Figure 4.3.

The instantaneous output power of the converter at time T_1 (i.e., the instant when the switch is turned OFF) is expressed as

$$P_1 = v_1 i_1 = P_R + P_{CPL}\,, \tag{4.2}$$

where $P_R = {v_1}^2/R$. The load power ratio a is defined such that

$$a = \frac{P_R}{P_1},\ \ (1-a) = \frac{P_{CPL}}{P_1}. \tag{4.3}$$

Assuming that the load values, R and P_{CPL}, remain constant during the switching interval (a fair assumption considering that the switching frequency is in the order of several kHz), the instantaneous output current of the converter at T_2 (i.e., the instant when the switch is turned ON at the beginning of the next switching cycle) can be expressed as

$$i_2 = \frac{v_2}{R} + \frac{P_{CPL}}{v_2}. \tag{4.4}$$

The load ratio a can then be computed based on (4.2)–(4.4) as

$$a = \frac{v_1(v_2 i_2 - v_1 i_1)}{i_1({v_2}^2 - {v_1}^2)}, \tag{4.5}$$

and the load values can be estimated as

$$R = \frac{v_1}{a i_1},\ \ P_{CPL} = (1-a) v_1 i_1\,. \tag{4.6}$$

It is worthwhile to point out a few implementation details pertaining to the proposed adaptive control method. First, the load estimation updates at every rising or falling edge of the gate signal; therefore, step changes in load (such as turning ON/OFF a resistive element) may result in erroneous prediction. Sharp load changes can be alleviated by comparing the output power

at consecutive sample times, and if the detected power change is large, the load will be set to pure CPL, resulting in the safest g calculation for that switching cycle in order to prioritize system stability. Once the transient is over, load estimation will be automatically corrected at the next switching cycle. Second, delay and other imperfections in signal sampling may affect the accuracy of load estimation; therefore, a sufficient safety margin should be considered in the calculation of g. Lastly, the load estimation technique works in variable and fixed-frequency operations, provided that the switching ripples can be sampled with reasonable accuracy given the resolution of the ADC. Constant switching frequency in SMC can be achieved through various methods (such as ramp signal injection) which will not be the focus here.

4.4 Performance Verification

To validate the effectiveness of the proposed adaptive SMC, a test scenario consisting of a series of load changes is devised using the converter system in Figure 4.2 with the parameters specified in Table 3.1. Recall that the same system and parameters were used in the stability boundary plot in Figure 4.1; hence, to help visualize the test scenario, Figure 4.4 zooms in on a relevant portion of Figure 4.1 and shows how the critical stability point of the system moves on the contour for each load change during the test scenario.

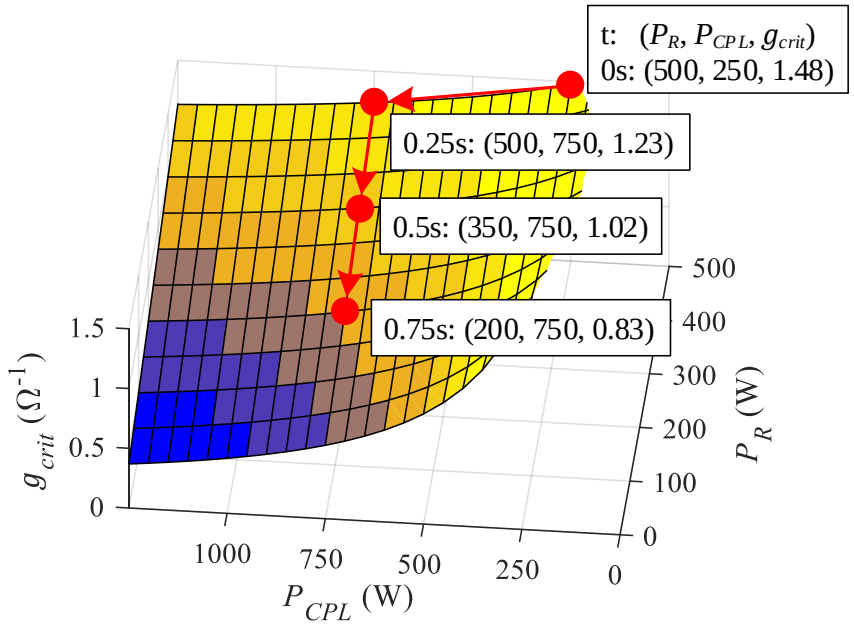

Figure 4.4 Local stability surface showing how g_{crit} shifts in the prescribed test scenario.

Here is a summary of the load changes during the test scenario:

- At t=0s, the system starts from steady-state, operating with a mix of 500W resistive load and 250W CPL. The critical g value is 1.48 at this operating point according to (4.1).
- At t=0.25s, the CPL power is increased to 750W at a slew rate of 20kW/s. The resistive load stays at 500W. g_{crit}=1.23 at this operating point.
- At t=0.5s, the resistive load is stepped down to 350W while the CPL power stays at 750W. g_{crit}=1.02 at this point.
- At t=0.75s, the resistive load is stepped down again to 200W while the CPL power stays at 750W. g_{crit}=0.83 at this point.

In addition, two conventional SM controllers using the fixed-g approach are used to compare with the proposed adaptive controller. One controller uses a fixed $g=0.3$ (calculated using the conservative stability condition (3.10) for the pure CPL case with 1250W CPL), and the other controller uses a fixed $g=0.9$ (calculated based on (4.1) for fast response around the operating point of 350W resistive and 750W CPL). The hysteresis band of the HC is set to 0.05 for all three controllers in the following simulation studies.

4.4.1 Simulation Results

Simulation results using MATLAB/Simulink are shown in Figure 4.5, in which (a) shows the load profile based on the test scenario in Figure 4.4, (b) shows the performance of the conventional SM controller with fixed $g=0.3$, (c) shows the performance of the conventional SM controller with fixed $g=0.9$, (d) shows the performance of the proposed adaptive SM controller with adjustable g and (e) shows the estimated load values using the proposed load estimation technique. Note that the estimated load values are used to calculate and update g in the proposed adaptive controller in Figure 4.5 (d).

As shown in Figure 4.5 (b), the conventional SM controller with fixed $g=0.3$ is stable during the test scenario but suffers slow response speed and large voltage dip during load transient. In Figure 4.5 (c), the conventional SM controller with fixed $g=0.9$ shows fast response speed during load changes at 0.25s and 0.5s but becomes unstable at 0.75s when g exceeds the critical value for that operating point. Lastly, in Figure 4.5 (d), the proposed adaptive SM controller exhibits fast response and is stable throughout the test scenario. The estimated load values using the proposed technique shown in Figure 4.5 (e) indicates good accuracy compared to the actual load profile in Figure 4.5 (a).

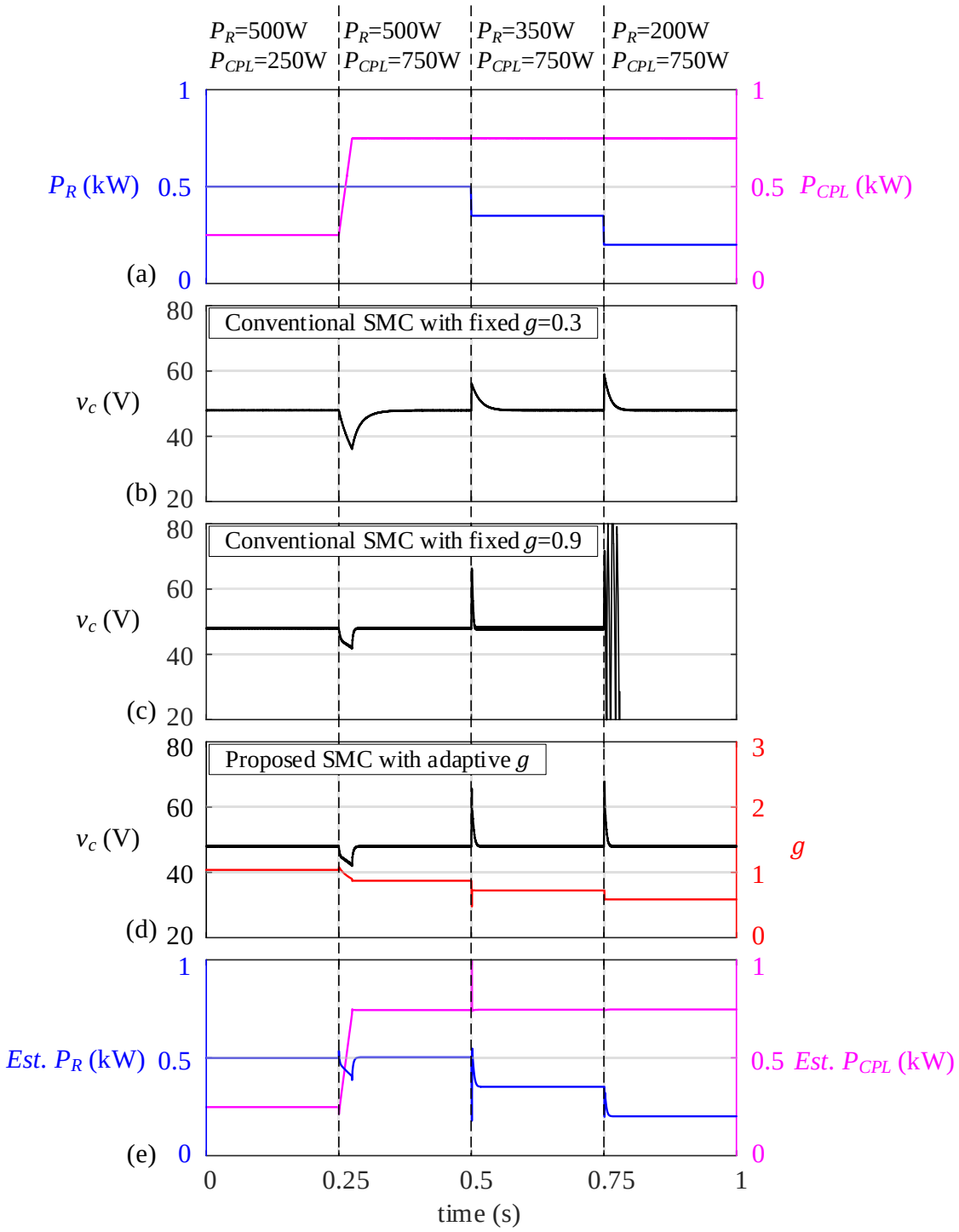

Figure 4.5 Simulation results showing dynamic performance of the boost converter driving mixed loads using conventional and proposed SM controllers.

4.4.2 Experimental Results Using Real-Time Simulator

Real-time hardware-in-the-loop (HIL) simulation is a fast-spreading technique adopted by both industry and academia in testing embedded systems [25]. HIL simulation also has a large presence in the power electronics industrial sector [25]. A HIL simulator offers an effective platform which encapsulates the complexities of a physical power converter system and allows safe, economic and efficient testing of the developed control. In this section, real-time HIL simulation with physical microcontroller unit (MCU) is used to validate the proposed adaptive control.

The proposed adaptive SM controller using adjustable g and load estimation algorithm (as shown in Figure 4.2), as well as the two fixed-g SM controllers, is implemented on a 32-bit MCU (TMS320F28335). Using digital interrupts, the switching frequency is fixed to 10kHz. The boost converter feeding resistive load and ideal CPL is implemented in the Typhoon HIL simulator (HIL602+). The programmed MCU is interfaced to the HIL simulator through analog and digital I/Os. The three SM controllers under study are then used to control the boost converter system on the HIL platform. The load changes prescribed in the test scenario (as shown in Figure 4.4) are automated in the HIL software interface (named “HIL SCADA”). The real-time experimental setup is shown in Figure 4.6.

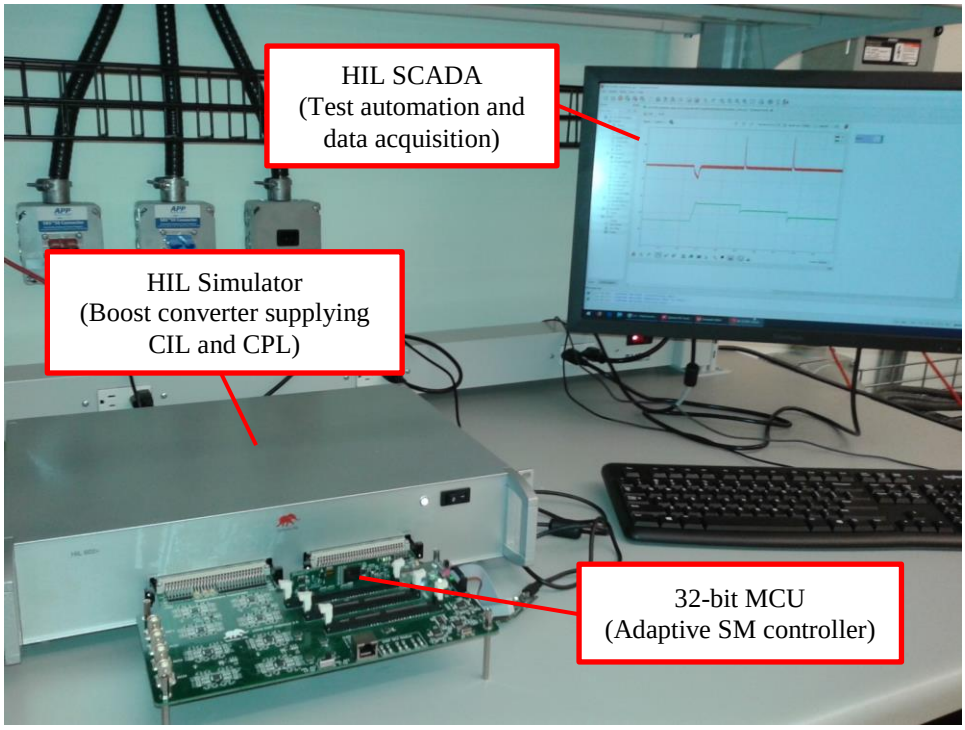

Figure 4.6 Experimental setup using DSP with the actual proposed controller and real-time HIL simulator.

The real-time simulation results are shown in Figure 4.7. As seen, the real-time results are consistent with the offline simulation results in Figure 4.5, again confirming the superior performance of the proposed adaptive control in terms of response speed and stability.

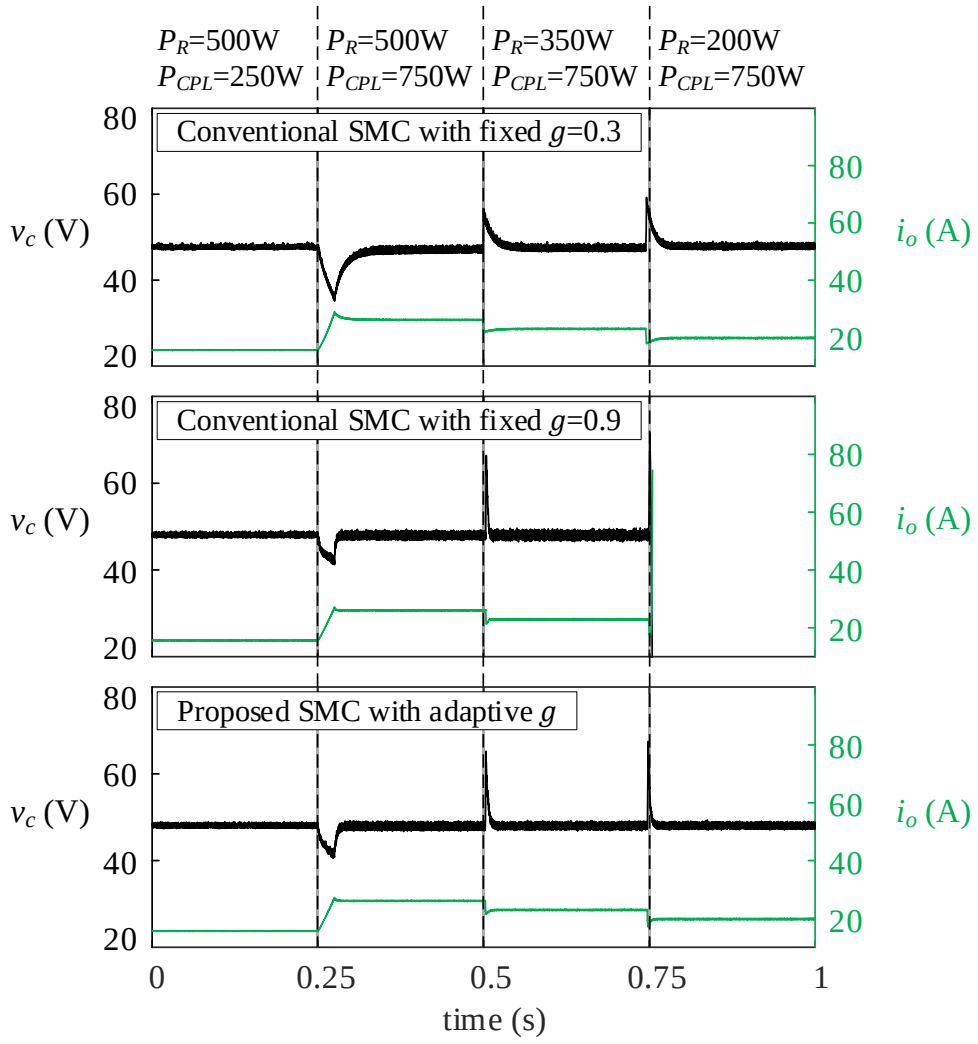

Figure 4.7 Experimental results of using DSP with the actual controller and real-time HIL simulator, showing dynamic performance of the boost converter driving mixed loads using conventional and proposed SM controllers.

4.5 Summary

In this chapter, a new adaptive sliding-mode control scheme using adjustable sliding coefficient and a load estimation technique has been proposed. Extensive simulation studies and experiments using DSP with the actual controller and real-time simulator have been carried out to validate the effectiveness of the proposed control. It has been demonstrated that the proposed control outperforms the conventional methods and achieves fast dynamic response while preserving system stability.

Chapter 5: Conclusions and Future Work

A strong, healthy DC bus is the backbone of any DC system. As today's DC systems become more prevalent and more complex, control of the bus-forming DC–DC boost converter becomes more challenging as the converter must withstand source fluctuations as well as load behaviors that have destabilizing effect. With the goal to design high-performance controllers for boost converters, this thesis capitalizes on the advantages of sliding-mode control and develops new control strategies that have shown to achieve very fast dynamic response with guaranteed stability.

5.1 Contributions

The core contribution of this work is that it advances the research on sliding-mode control in its application to the control of boost converters, offering both extensible analytical framework and practical techniques for controller design and implementation. The detailed contributions are identified along with a summary of each of the three research objectives.

Objective 1 is achieved in Chapter 2, in which an observer-based sliding-mode controller is developed for boost converters supplying constant impedance load, resulting in a significant performance improvement with the addition of only a voltage sensor. The new observed-based control strategy is extensible to other basic topologies and is useful in designing ultrafast converters driving simple loads for improved efficiency and reliability.

Objective 2 is achieved in Chapter 3, in which the basic sliding-mode framework has been extended to controlling boost converters supplying both constant impedance and constant power

loads. A systematic approach for analyzing system dynamics and stability under sliding-mode control has been presented. An accurate closed-loop small-signal model for the highly-nonlinear mixed-load system has been developed for the first time. The analytical approach to system stability and the methodology for deriving the linearized closed-loop small-signal model and system transfer functions should be applicable to other, possibly higher-order, topologies under sliding-mode control.

Objective 3 has been achieved in Chapter 4, in which a new adaptive sliding-mode controller for boost converters supplying both constant impedance and constant power loads has been proposed and developed in full detail. The new control strategy utilizes the stability findings from Objective 2 and automatically tunes the control parameter to achieve fast response and stable performance. An innovative load estimation technique based on output switching ripple has also been developed and presented in detail. Since switching ripple is inherent to all DC–DC converters, the proposed load estimation technique is anticipated to have great potential in load identification in general.

5.2 Future Work

In this thesis, the DC system and its major components have been simplified and generalized so that the analysis and control methods presented here can be applied broadly to other topologies and systems. With this in mind, future research can continue in the following directions:

It would be very desirable to extend the presented sliding-mode control framework to other widely-used bus-forming converter topologies such as bidirectional boost, cascaded buck-boost and so on. System dynamics and stability can be analyzed using the systematic approach along the

lines presented in this thesis. Moreover, the concept of adaptive sliding-mode control presented in Chapter 4 should be applicable to other converter topologies as well.

Another important future research direction is to model and analyze the system in greater detail including parasitic elements and control bandwidth limitations of the source and load converters, including a non-ideal constant power load. Furthermore, the adaptive sliding-mode controller and the load estimation algorithm presented in Chapter 4 could be modified and improved to work with downstream converter/inverter loads whose input waveforms are discontinuous.

Bibliography

[1] A. P. N. Tahim, D. J. Pagano, E. Lenz and V. Stramosk, "Modeling and stability analysis of islanded DC microgrids under droop control," *IEEE Trans. Power Electron.*, vol. 30, no. 8, pp. 4597–4607, Aug. 2015.

[2] A. Emadi, A. Khaligh, C. H. Rivetta and G. A. Williamson, "Constant power loads and negative impedance instability in automotive systems: definition, modeling, stability, and control of power electronic converters and motor drives," *IEEE Trans. Veh. Technol.*, vol. 55, no. 4, pp. 1112–1125, Jul. 2006.

[3] R. W. Erickson and D. Maksimovic, *Fundamentals of Power Electronics*. Norwel, MA, USA: Kluwer, 2001.

[4] L. Guo, J. Y. Hung and R. M. Nelms, "Evaluation of DSP-based PID and fuzzy controllers for DC–DC converters," *IEEE Trans. Indust. Electron.*, vol. 56, no. 6, pp. 2237–248, Jun. 2009.

[5] S. Singh, A. R. Gautam and D. Fulwani, "Constant power loads and their effects in DC distributed power systems: a review," *Renew. Sustain. Energy Rev.*, vol. 72, pp. 407–421, May 2017.

[6] E. Hossain, R. Perez, A. Nasiri and S. Padmanaban, "A comprehensive review on constant power loads compensation techniques," *IEEE Access*, vol. 6, pp. 33285–33305, Jun. 2018.

[7] P. Mattavelli, L. Rossetto, G. Spiazzi and P. Tenti, "General-purpose fuzzy controller for DC-DC converters," *IEEE Trans. Power Electron.*, vol. 12, no. 1, pp. 79–86, Jan. 1997.

[8] P. Mattavelli, L. Rossetto, G. Spiazzi and P. Tenti, "General-purpose sliding-mode controller for DC/DC converter applications," in *Proc. IEEE Power Electronics Specialist Conf. - PESC '93*, Seattle, WA, USA, pp. 609–615, 1993.

[9] S. Tan, Y. M. Lai and C. K. Tse, "A unified approach to the design of PWM-based sliding-mode voltage controllers for basic DC-DC converters in continuous conduction mode," *IEEE Trans. Circuits and Systems I: Regular Papers*, vol. 53, no. 8, pp. 1816–1827, Aug. 2006.

[10] V. Utkin, "Variable structure systems with sliding modes," *IEEE Trans. Automatic Control*, vol. 22, no. 2, pp. 212–222, Apr. 1977.

[11] G. Spiazzi and P. Mattavelli, "Sliding-mode control of switched-mode power supplies," *The Power Electronics Handbook*. Boca Raton, FL: CRC, 2002, Ch. 8.

[12] S. Tan, Y. M. Lai, C. K. Tse, L. Martinez-Salamero and C. Wu, "A fast-response sliding-mode controller for boost-type converters with a wide range of operating conditions," *IEEE Trans. Indust. Electron.*, vol. 54, no. 6, pp. 3276–3286, Dec. 2007.

[13] S. Tan, Y. M. Lai and C. K. Tse, "Indirect sliding mode control of power converters via double integral sliding surface," *IEEE Trans. Power Electron.*, vol. 23, no. 2, pp. 600–611, Mar. 2008.

[14] S. Tan, Y. M. Lai, C. K. Tse and M. K. H. Cheung, "Adaptive feedforward and feedback control schemes for sliding mode controlled power converters," *IEEE Trans. Power Electron.*, vol. 21, no. 1, pp. 182–192, Jan. 2006.

[15] S. Tan, Y. M. Lai and C. K. Tse, "General design issues of sliding-mode controllers in DC–DC converters," *IEEE Trans. Indust. Electron.*, vol. 55, no. 3, pp. 1160–1174, Mar. 2008.

[16] E. Vidal-Idiarte, A. Marcos-Pastor, R. Giral, J. Calvente and L. Martinez-Salamero, "Direct digital design of a sliding mode-based control of a PWM synchronous buck converter," *IET Power Electron.*, vol. 10, no. 13, pp. 1714–1720, Oct. 2017.

[17] R. K. Subroto, L. Ardhenta and E. Maulana, "A novel of adaptive sliding mode controller with observer for DC/DC boost converters in photovoltaic system," in *Proc. 5th International Conf. Electrical, Electronics and Information Engineering (ICEEIE)*, Malang, pp. 9–14, 2017.

[18] P. Mattavelli, L. Rossetto and G. Spiazzi, "Small-signal analysis of DC–DC converters with sliding mode control," *IEEE Trans. Power Electron.*, vol. 12, no. 1, pp. 96–102, Jan. 1997.

[19] S. Singh, D. Fulwani and V. Kumar, "Robust sliding-mode control of dc/dc boost converter feeding a constant power load," *Power Electron. IET*, vol. 8, no. 7, pp. 1230–1237, Jul. 2015.

[20] B. A. Martinez-Treviño, A. El Aroudi, E. Vidal-Idiarte, A. Cid-Pastor and L. Martinez-Salamero, "Sliding-mode control of a boost converter under constant power loading conditions," *Power Electron. IET*, vol. 12, no. 3, pp. 521–529, Mar. 2019.

[21] A. P. N. Tahim, D. J. Pagano and E. Ponce, "Nonlinear control of dc-dc bidirectional converters in stand-alone dc microgrids," in *Proc. IEEE 51st Conf. Decision Control*, pp. 3068–3073, Dec. 2012.

[22] W. Jiang, X. Zhang, F. Guo, J. Chen, P. Wang and L. H. Koh, "Large-Signal Stability of Interleave Boost Converter System With Constant Power Load Using Sliding-Mode Control," *IEEE Trans. Indust. Electron.*, vol. 67, no. 11, pp. 9450-9459, Nov. 2020.

[23] E. B. Braiek and F. Rotella, "Design of observers for nonlinear time variant systems," in *Proc. IEEE Systems Man and Cybernetics Conf. - SMC*, Le Touquet, France, pp. 216–220, 1993.

[24] F. Auger, M. Hilairet, J. M. Guerrero, E. Monmasson, T. Orlowska-Kowalska and S. Katsura, "Industrial applications of the Kalman filter: A review," *IEEE Trans. Indust. Electron.*, vol. 60, no. 12, pp. 5458–5471, Dec. 2013.

[25] (2020) Typhoon HIL Customer Archive. [Online]. Available: https://www.typhoon-hil.com/customer/

[26] V. Utkin, J. Guldner, and J. Shi, *Sliding Mode Control in Electro-Mechanical Systems*, 2nd ed. Boca Raton, FL, USA: CRC Press, 2009.

[27] L. Martinez-Salamero, A. Cid-Pastor, R. Giral, J. Calvente, and V. Utkin, "Why is sliding mode control methodology needed for power converters?" in *Proc. 14th Int. EPE/PEMC*, pp. S9-25–S9-31, Sep. 2010.

[28] J. Ackermann and V. Utkin, "Sliding-mode control design based on Ackermann's formula," *IEEE Trans. Autom. Contr.*, vol. 43, no. 2, pp. 234–237, Feb. 1998.

[29] P. Mattavelli, "Digital control of DC-DC boost converters with inductor current estimation," in *Proc. IEEE Appl. Power Electron. Conf. Expo.*, vol. 1, pp. 74–80, 2004.

[30] A. P. Tahim, D. J. Pagano, M. L. Heldwein, and E. Ponce, "Control of interconnected power electronic converters in dc distribution systems," in *Proc. Brazilian Power Electron. Conf. (COBEP)*, pp. 269–274, Sep. 2011.

[31] J. Wu and Y. Lu, "Adaptive backstepping sliding mode control for boost converter with constant power load," *IEEE Access*, vol. 7, pp. 50797–50807, 2019.

[32] (2020). MathWorks Documentation. [Online]. Available: https://www.mathworks.com/.

[33] (2019). TMS320F2833x, TMS320F2823x Digital Signal Controllers (DSCs) datasheet Rev. O, Texas Instruments. [Online]. Available: https://www.ti.com/lit/ds/sprs439o/sprs439o.pdf

[34] (2020). TMS320x2833x, TMS320x2823x Technical Reference Manual, Texas Instruments. [Online]. Available: https://www.ti.com/lit/ug/sprui07/sprui07.pdf

[35] (2020). Typhoon HIL Documentation. [Online]. Available: https://www.typhoon-hil.com/documentation/